Dynamic Compression and Volatile Release of Carbonates

James A. Tyburczy and Thomas J. Ahrens

Seismological Laboratory

California Institute of Technology

Pasadena, CA 91125

Revised November 13, 1984

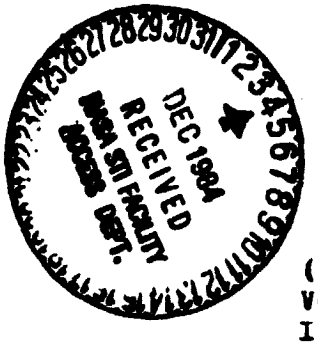

ABSTRACT

Particle velocity profiles upon shock compression and isentropic release were measured for polycrystalline calcite (Solenhofen limestone) to 12 to 24 GPa and for porous calcite (Dover chalk, ρ_o = 1.40 g/cm^3, 49% porosity) to between 5 and 11 GPa. The electromagnetic particle velocity gauge method was used. Upon shock compression of Solenhofen limestone, the Hugoniot elastic limit was determined to vary from .36 to .45 GPa. Transition shocks at between 2.5 and 3.7 GPa, possibly arising from the calcite II-III transition, were observed. For the Solenhofen limestone, the release paths lie relatively close to the Hugoniot. Evidence for the occurrence of the calcite III-II transition upon release was observed, but no rarefaction shocks were detected. Initial release wave speeds suggest retention of shear strength up to at least 20 GPa, with a possible loss of shear strength at higher pressures. The measured equation of state is used to predict the fraction of material devolatilized upon isentropic release as a function of

shock pressure. The effect of ambient partial pressure of CO_2 on the calculations is demonstrated and should be taken into account in models of atmospheric evolution by means of impact-induced mineral devolatilization. Mass fractions of CO_2 released expected on the basis of a continuum model are much lower than determined experimentally. This discrepancy, and radiative characteristics of shocked calcite indicate that localization of thermal energy (shear banding) occurs under shock compression. Release isentrope data indicates that Dover chalk loses its shear strength when shocked to 10 GPa pressure. At 5 GPa the present data are ambiguous regarding possible shear strength. For Dover chalk, shock entropy calculations result in a minimum estimate of 90% devolatilization upon complete release from 10 GPa. Isentropic release paths from calculated continuum Hugoniot temperatures cross into the CaO (solid) + CO_2 (vapor) field at improbably low pressures (for example 10^{-7} GPa for a shock pressure of 25 GPa). However, release paths from measured shock temperatures cross into the melt plus vapor field at pressures greater than .5 GPa, suggesting that devolatilization is initiated at the shear banding sites.

Introduction

The shock compression and release behavior of carbonates is of interest in the study of cratering mechanics, shock metamorphism in carbonate terranes and the generation of CO_2 bearing atmospheres on the terrestrial planets. Approximately 30% of the known or probable terrestrial meteorite impact craters occur at least partially in carbonate rocks [Grieve and Robertson, 1979]. Impact-induced devolatilization of hydrous and carbonate minerals appears to play a role in the evolution of terrestrial planetary atmospheres [Lange and Ahrens, 1983, 1984].

Static compression studies indicate that two metastable polymorphs of calcite ($CaCO_3$), exist at pressures above that of the calcite-aragonite transition (Bridgman, 1939; Jamieson, 1957). The single crystal calcite Hugoniot shows density discontinuities at pressures of between 1.8 to 2.4 GPa, at about 3 GPa, at about 4.5 GPa, and at about 9.5 GPa, corresponding to the Hugoniot elastic limit (HEL) and the calcite I-II, II-III, and III-VI (see below) transitions, respectively [Ahrens and Gregson, 1964]. Analogous transitions occur in shocked limestone (polycrystalline calcite), although at somewhat lower pressures [Ahrens and Gregson, 1964, Grady *et al.*, 1978]. The aragonite Hugoniot also displays evidence of several transitions [Vizgirda and Ahrens, 1982], which are probably unrelated to calcite II and III since aragonite is denser than these phases. Above about 10 GPa the single crystal calcite [Ahrens and Gregson, 1964], polycrystalline calcite [Adadurov *et al.*, 1961; Kalashnikov *et al.*, 1973; van Thiel *et al.*, 1977], and single crystal aragonite [Vizgirda and Ahrens, 1982] Hugoniots are very similar, suggesting transformation to a similar high pressure polymorph above that pressure. In the remainder of the text we refer to this stable high pressure polymorph as calcite VI. Calcite IV and V are low-pessure, high-temperature forms of $CaCO_3$ [Carlson, 1983].

Release isentropes for polycrystalline calcite rocks shocked to pressures up to about 4 GPa have been determined using laser interferometry [Schuler and Grady, 1977; Grady *et al.*, 1978; Grady, 1983] and electromagnetic particle velocity gauges [Larson and Anderson, 1979]. Murri *et al.* [1975] employed electromagnetic particle velocity gauges to determine release paths for selected carbonate rocks (porosity 0 and 15%) shocked to between 10 and 30 GPa. In this pressure range the initial release paths lie at greater densities than the Hugoniot. Release paths for single crystal aragonite shocked to pressures up to 40 GPa have been determined using buffer and inclined mirror techniques [Vizgirda and Ahrens, 1982]. For shock pressures up to about 13 GPa the release paths are steep, and maximum post-shock densities are greater than the initial volume. For shock pressures, between about 13 and 40 GPa the release paths generally lie close to the Hugoniot, and maximum post-shock densities are less than or equal to the initial density.

Shock loaded calcite decarbonates (i.e., decomposes to CaO plus CO_2 gas) when shocked to pressures as low as 10 GPa [Lange and Ahrens, 1983, 1984]. However, calculations of post-shock energy content assuming that the release path is identical to the Hugoniot require a shock pressure of 45 GPa for incipient devolatilization [Kieffer and Simonds, 1980], and consideration of post-shock entropy content assuming isentropic release [Zel'dovich and Raizer, 1967; Ahrens and O'Keefe, 1972] requires shock pressures of 33 GPa for incipient devolatilization [Vizgirda and Ahrens, 1982]. However, these previous applications of post-shock energy and entropy calculations have failed to consider the effect of the ambient partial pressure of the volatile species on the equilibrium of the devolatilization reaction.

A shock temperature measurement at 40 GPa on single crystal calcite yields a color temperature of 3700 K, which is over twice the Hugoniot

temperature calculated from continuum thermodynamic models, with an emissivity of 0.0025 [Kondo and Ahrens, 1983]. This result has been interpreted as indicating the presence of a large number of closely spaced high temperature shear-band regions immediately behind the shock front, in support of the shear instability models of Grady [1977, 1980] and Horie [1980]. These zones of intense heating would cause devolatilization to begin at much lower pressures than those calculated on the basis of continuum models.

In an effort to determine the limits of applicability of continuum models, we have determined the release paths for a slightly porous polycrystalline carbonate (Solenhofen limestone, ρ_o = 2.58 g/ cm^3) shocked to pressures between 12 and 24 GPa and for a very porous calcite (Dover chalk, ρ_o = 1.40 g/ cm^3) shocked to between 5 and 11 GPa pressure using the electromagnetic particle velocity gauge technique. Release paths have not been previously determined for these materials shocked to these pressures. The release path data are used to determine the post-shock energy gain which is then compared to estimated values of energy input required for incipient volatilization E_{IV}. In addition, the sound velocity data obtained for the shocked state and along the unloading path provide constraints on the mechanical strength properties of these materials during shock compression and unloading.

Experimental Technique

The particle velocity gauge technique used in these experiments is described elsewhere in detail [Boslough, 1983], and shown schematically in Figure 1. The targets consisted of four 1.5 mm thick plates of Solenhofen limestone with 12.5 μm thick copper, polyamide-backed (Kapton, 12.5 μm) particle velocity gauges epoxied between each plate and onto the free surface. The faces of the assembled target were parallel to within 25 μm. Archimedean and bulk densities were determined individually for each plate. The chalk target assemblies

are shown in Figure 2. In the chalk assemblies the gauges were stretched across each plate and epoxied only on a 3 mm wide strip along the plate edge. Because the chalk is relatively weak, each target assembly consisted of only three 2 to 2.5 mm thick plates. Additional clamping was provided by a circular clamp ring on the front and clamping strips on the rear of the mounting ring.

The target was mounted at the center of a set of Helmholtz coils so that the active element of each gauge, the incident projectile velocity, and the magnetic field generated by the coils were mutually perpendicular. Upon impact a voltage is induced across the active element of the gauge which is proportional to the effective gauge (active element) length L, the magnetic induction B, and the particle velocity u_p,

$$V(t) = B\,L\,u_p(t) \qquad (1)$$

where t is the time after impact. V(t) is in units of volts when B is in gauss, L is in cm, and u_p is in cm/sec. In these experiments B was approximately 1.8 kG and L was approximately 0.95 cm. The gauge voltages were recorded by a series of 4 Tektronix oscilloscopes using the circuits sketched in Fig. 3.

The shots were performed on the 40 mm propellant gun at the California Institute of Technology [Ahrens *et al.*, 1971]. The impact tank pressure was between 50 and 160 μm Hg. Fused quartz and polycrystalline alumina flyer plates between 6 and 18 mm thick were employed. The projectile velocity was measured by determining the flight distance of the projectile during the known time interval between two flash x-ray photographs of the projectile.

Typical experimental results are shown in Figure 4, which shows particle velocity versus time after impact obtained from digitized oscilloscope records. The shock wave generated by the impact reaches each of the gauges in sequence (gauge 1 is nearest the impacted surface, gauge 4 is on the rear, or free,

surface) accelerating it to the particle velocity of the Hugoniot state. Gauge 4 is accelerated immediately to the free surface velocity. Gauge 3 and then gauge 2 are later accelerated to higher particle velocities by the rarefaction wave propagating back into the sample from the free surface. Gauge 2 is disrupted by rarefactions originating at the edges of the target before reaching the final free surface velocity. Gauge 1 is intercepted by the forward-travelling rarefaction originating at the upstream side of the flyer plate and is therefore accelerated to lower particle velocities. These relationships are shown more clearly in schematic position-time plot, shown in Figure 5.

The time interval between the shock arrival at each gauge was used to determine the shock wave velocity. This was combined with the projectile velocity and the known flyer material Hugoniot [Marsh, 1980] in an impedance match solution [McQueen *et al.*, 1970] to yield the Hugoniot state. The Hugoniot particle velocity obtained in this way provided the reference point for the gauge voltage versus particle velocity calibration.

The stress and density along the release path are given by equations for conservation of mass and linear momentum [Cowperthwaite and Williams, 1971]

$$\left(\partial \rho / \partial u_p\right)_h = \frac{\rho^2}{\rho_o} C_u \tag{2}$$

$$\left(\partial \sigma / \partial u_p\right)_h = \rho_o C_\sigma \tag{3}$$

where ρ is the density, ρ_o is initial density, u_p is particle velocity, h is the Lagrangian space coordinate, and

$$C_u = (\partial h / \partial t)_u \tag{4a}$$

$$C_\sigma = (\partial h / \partial t)_\sigma \tag{4b}$$

where t is time. C_u is the velocity of propagation of a wave with particle velocity u_p, and C_σ is the velocity of propagation of a wave with stress σ. The release waves are nonsteady simple waves [Courant and Friedrichs, 1948; Petersen *et al.*, 1970] Therefore C_u and C_σ are equal, but depend on u_p. The digitized particle velocity as a function of time records were used to compute C_u and then equations (2) and (3) were integrated numerically to obtain the stress-density path of the release. The Lagrangian sound speed, C_u, is obtained using the finite difference approximation,

$$C_u \approx \frac{\Delta h}{\Delta t} \tag{5}$$

where Δh is the initial distance between gauges and Δt is the transit time for a disturbance with a particle velocity u_p. Eulerian sound speeds are equal to

$$C_E = \frac{\rho_o}{\rho} C_u \tag{6}$$

The Eulerian sound speed corresponds to the sound speed relative to the laboratory reference frame.

Results

The experimental results for the shocked states of the Solenhofen limestone and the Dover chalk are summarized in Table 1. Figures 6 and 7 are shock velocity-particle velocity (U_s–u_p) and pressure-density (P-ρ) plots of the data, respectively. The experimental data for shot 599 (Dover chalk) appear to be erroneous. The results are listed in Table 1, but are not plotted. No release path data were obtained from shot 601.

In two of the shots, shots 596 and 602 (Hugoniot pressures 13.10 and 11.96 GPa, respectively), multiple wave structure was observed (Figure 8). Transitions occurring between .36 and .45 GPa and between 2.5 and 3.7 GPa were identified.

Multiple wave structure has been observed in previous shock wave experiments on carbonates, and is caused by dynamic yielding and at least 3 additional phase changes that calcite undergoes at low pressures [Ahrens and Gregson, 1964; Grady *et al.*, 1978]. However, in the experiments reported here the shock and particle velocities of the intermediate states are poorly constrained, and are not completely consistent. These less reliable data are shown in parentheses in Table 1.

The velocity of 5.7 ± 0.3 km/sec for the first wave of shot 602 (Table 1) is comparable to the longitudinal wave velocity of Solenhofen limestone, 5.84 - 5.97 km/sec [Peselnick, 1962; Hughes and Cross, 1951] indicating that this transition represents the Hugoniot elastic limit (HEL). Ahrens and Gregson [1964] report elastic precursor velocities of 5.3 to 5.7 km/sec and a HEL of 1.0 to 1.5 GPa for carbonate-bearing rocks. Grady *et al.* [1978] report a break in the Solenhofen limestone loading wave profile at 0.6 GPa and conclude that the calcite I-II phase transition occurs at this pressure, coincident with the onset of dynamic yielding. Our data are not of sufficient resolution in this pressure range to resolve this question. Comparison with the results of Grady *et al.* [1978] suggests that the transition at 2.5 to 3.7 GPa corresponds to the calcite II-III transition. In the higher shock pressure shots these transitions are apparently overdriven, in agreement with previous shock experimental results [Ahrens and Gregson, 1964]. No precursory waves were observed in the shots on Dover chalk.

Figure 6 shows the U_s–u_p data determined in this study compared to trends observed in various calcium carbonate-bearing rocks and minerals by previous investigators. For Solenhofen limestone the values of U_s and u_p lie within the range of values previously determined by other investigators, but the slope of the line defined by the data is greater. The data in the range of 12 to 24 GPa can be fit by an equation of the form

$$U_s = C_o + s\,u_p \qquad (7)$$

where C_o and s are constants, with C_o = 3.269 km/sec and s = 1.796 (r^2 = 0.97). Previously determined values of C_o and s range from 3.62 to 3.99 km/sec and 1.32 to 1.61, respectively, and are summarized in Table 2. The U_s–u_p data for Dover chalk, ρ_o = 1.40 g/cm^3, can be fit with C_o = 0.667 and s = 1.538 (r^2 = 0.989). This line is consistent with the trend formed by the porous calcite results of Kalashnikov *et al.*, [1973].

As shown in Figures 4 and 8, the particle velocity records of all the Solenhofen limestone shots indicate that a phase transition occurs upon release. The pressures and densities at which it occurs for each shot are listed in Table 1. The data are somewhat scattered but the transition occurs at about 5.5±2.5 GPa, and no trend with peak stress level is apparent. Previous observations of a phase transition upon release in this pressure range have been attributed to the calcite III-II transition [Grady *et al.*, 1978]. Rarefaction shocks have been observed in carbonates shocked to these pressures [Murri *et al.*, 1975]. However, no evidence for rarefaction shocks was seen in these experimental records.

The initial release paths for Solenhofen limestone plotted in Figure 7 lie near the Hugoniot, but at slightly higher densities, for all shock pressures studied. The particle velocity records do not give complete information down to zero pressure due to disruption of the foil gauges by rarefactions propagating inward from the sample edges. Extrapolation to zero-pressure yields complete release densities between 2.59 and 2.81 g/cm^3. In contrast to the behavior for Solenhofen limestone, release paths for single crystal aragonite vary significantly with shock pressure. For shock pressures between about 10 and 15 GPa the aragonite release paths are very steep, with complete release densities (determined via inclined mirror experiments) equal to or greater than the initial

density. For shock pressures greater than about 20 GPa, the release paths approximate the Hugoniot, with complete release densities equal to or less than the initial density [Vizgirda and Ahrens, 1982]. Release paths for Solenhofen limestone [Schuler and Grady, 1977] and other carbonate rocks [Grady *et al.*, 1976; Grady, 1983] shocked to pressures up to about 5 GPa generally follow the Hugoniot, with extrapolated complete release densities approximately equal to the initial density.

The release paths for Dover chalk lie at higher densities than the Hugoniot. The extrapolated complete release densities lie between 2.44 and 2.55 g/cm^3.

Eulerian sound speeds for the shocked states were calculated according to equations 5 and 6 and are plotted in Figure 9.

Discussion

Properties of calcite VI, reached at about 10 GPa shock pressure, have been deduced by Vizgirda and Ahrens [1982] and are listed in Table 3. The zero-pressure bulk sound velocity

$$V_\phi = (K_{os}/\rho_o)^{1/2} \tag{8}$$

where K_{os} is the zero pressure isentropic bulk modulus, is between about 5.00 and 5.54 km/sec at 300 K. Assuming a Poisson's ratio σ of 0.25 we obtain a zero-pressure, 300 K compressional velocity V_p of between 6.46 and 7.15 km/sec using the relationship

$$V_p = \left\{K_{os}/\rho\cdot[1+2\,(1-2\sigma)/(1+\sigma)]\right\}^{1/2} \tag{9}$$

We can compare the observed Hugoniot sound velocities with compressional wave velocities V_p along an isentrope for calcite VI using finite strain-theory [Sammis *et al.*, 1970; see also Burdick and Anderson, 1975]. Thus,

$$V_p^2(\rho) = V_{p,o}^2 (1-2\varepsilon)[1-2\varepsilon(3D_p - 1)] \quad (10)$$

$$V_s^2(\rho) = V_{s,o}^2 (1-2\varepsilon)[1-2\varepsilon(3D_s - 1)] \quad (11)$$

and

$$P = -3K_{oo}\,\varepsilon\,(1-2\varepsilon)^{5/2}\,(1+2\varepsilon\,\xi). \quad (12)$$

The volumetric strain ε is

$$\varepsilon = [\,1 - (\rho/\rho_o)^{2/3}\,]/2 \quad (13)$$

the finite strain parameter ξ is

$$\xi = 3[4 - (d\,K_{oo}/dP)_s]/4 \quad (14)$$

$$D_p = K_{oo}\,d\,ln\,V_p/d\,P \quad (15)$$

and

$$D_s = K_{oo}\,d\,ln\,V_s/d\,P \quad (16)$$

No determinations of D_p and D_s for calcite VI exist. For many minerals D_p lies in the range $1.0 \leq D_p \leq 1.6$ and D_s lies between $0.1 \leq D_s \leq 1.0$ [Anderson *et al.*, 1968; Sammis *et al.*, 1970]. This range of values was used in computing $V_p(\rho)$ and $V_s(\rho)$. The variation of bulk sound speed V_ϕ along an isentrope is given by

$$V_\phi^2(\rho) = V_p(\rho)^2 - 4\,V_s^2(\rho)/3 \quad (17)$$

The effect of temperature on sound velocity is small. The temperature along the Hugoniot T_H was calculated using continuum methods [Zel'dovich and Raizer, 1967] and is listed for each shot in Table 4. The parameters used for the calculation of T_H are listed in Table 3. For the Dover chalk, the temperatures

are sufficiently high that calculated Hugoniot temperatures are relatively insensitive to the specific isentrope employed in the calculation. Assuming a value of $(d V_p/ dT)_p$ of -3.3×10^{-4} km/ sec · K (values tabulated by Anderson *et al.* [1968] range from about -1.5×10^{-4} to -5.2×10^{-4} km/ sec · K), an increase in the initial temperature of 450 K results in a V_p decrease of 0.15 km/sec.

The range of values of V_p and V_ϕ along a 750 K isentrope calculated using the parameters listed in Table 3 is shown in Figure 9. Although the calculated bulk and compressional sound speeds are poorly constrained, the data indicate that the measured initial release wave speed is equal to that of the compressional wave velocity for shock pressures up to about 20 GPa. In other words, calcite VI retains its shear strength in the shocked state up to this pressure. At the highest pressures attained, 22 to 24 GPa, a loss of strength in the shocked state may occur.

The bulk sound speed V_ϕ at the Hugoniot may also be calculated from the shock wave equation of state (equation (7)) and a model for the Gruneisen parameter γ, using the relationship

$$V_\phi = V_H \left\{ \frac{dP}{dV}\Big|_H \left[(V_o - V_H) \frac{\gamma}{2V_H} - 1 \right] + P_H \gamma / 2V_H \right\}^{1/2} \qquad (18)$$

[McQueen *et al.*, 1967] where V_o is the initial sample volume, V_H is the Hugoniot volume, and $\frac{dP}{dV}\Big|_H$ is the slope of the Hugoniot. We use the relationship $\gamma = \gamma_o (\rho_o / \rho)$ where $\gamma_o = 1.5$ and $n = 1.0$ [Vizgirda & Ahrens, 1982] (Table 3). This curve is plotted as a dashed line in Figure 9 and supports the conclusion that a loss of shear strength occurs at a pressure of 22 to 24 GPa.

The Eulerian sound speeds along the release paths of the shocked Dover chalk are plotted in Figure 10. At the relatively low shock pressures and high continuum temperatures reached in these experiments it is unlikely that the

starting material transformed to calcite VI. However, it is not known which of the three calcite low pressure polymorphs exists in the shocked state. We have therefore plotted the bulk and compressional wave velocities for calcite I, II, and III using, for comparison, the data of Singh and Kennedy [1974], assuming that Poisson's ratio $\sigma = 0.25$ [Anderson *et al.*, 1968; Grady *et al.*, 1978]. Also plotted is the bulk sound speed in the shocked state calculated using the low pressure (5-13 GPa) polycrystalline calcite Hugoniot of Adadurov *et al.* [1961] and equation (18). The datum for shot 620 plots between the bulk and compressional wave velocities for calcite I and III, whereas the result for shot 622 (P_H = 9.47 GPa) lies near the bulk sound speed of calcite I and III.

The behavior observed for the limestone and chalk may be compared with observations on other minerals. San Gabriel anorthosite shocked to pressures between 6 and 10 GPa retains its shear strength in the shocked state, but undergoes a strength loss upon release [Boslough and Ahrens, 1984]. Quartz shocked into the mixed-phase region [Grady *et al.*, 1975] and non-porous carbonates at shock pressures up to about 5 GPa [Grady *et al.*, 1978] have initial release wave speeds equal to the bulk sound speed. There appear to be two mechanisms that cause loss of shear strength in the shocked state. The onset of shear strength loss occurs upon the initiation of phase transition. Thus, materials undergoing phase transitions along the Hugoniot (quartz, carbonates at low pressure) exhibit initial release wave velocities equal to bulk sound speed, whereas materials undergoing transformation upon release (carbonates above 10 GPa shock pressure, anorthosite) exhibit initial release wave velocities corresponding to compressional wave speed, with a reduction to lower velocities upon release. Shear strength loss also accompanies extensive shear band formation [Grady *et al.*, 1975]. At 22 GPa Solenhofen limestone exhibits a loss of shear strength. At this shock pressure, the measured shock temperature is approximately 2455 K

(D. Schmitt, personal communication), over twice the calculated continuum temperature. Apparently, at this shock pressure the shear band density is large enough to affect the bulk material properties.

Shock recovery experiments on single crystal calcite demonstrate that the onset of decarbonation according to the reaction

$$CaCO_{3(s)} \xrightarrow[\text{impact}]{} CaO_{(solid)} + CO_{2\,(gas)} \tag{19}$$

occurs upon release from shock pressures of less than 10 GPa (Lange and Ahrens, 1983). Upon complete release from 12-13 GPa shock pressure, about 30 per cent of the CO_2 initially present is volatilized, and 50-60 per cent of the CO_2 is lost upon release from 20-25 GPa [Lange & Ahrens, 1983]. In the following sections we compare the experimentally determined values of the fraction of CO_2 volatilized with calculations based on post-shock energy and entropy content.

The post-shock energy increase ΔE_p in a material shocked to Hugoniot pressure P_H and volume V_H is given by [Ahrens and O'Keefe, 1972, Zel'dovich and Raizer, 1967]

$$\Delta E_p = E_p - E_o = \frac{1}{2}(P_o + P_H)(V_o - V_H) - \int_{V_H}^{V_{oo}} (PdV)_s \tag{20}$$

where E_p is the post-shock energy content, E_o is the initial energy content, V_o is the initial specific volume, and V_{oo} is the complete release volume. The integral is performed along the release path, which is assumed to be isentropic [Kieffer and Delaney, 1979; Jeanloz and Ahrens, 1979]. The first term on the right hand side of equation (20) is the internal energy increase upon loading the sample to the Hugoniot, and the second term represents the work performed in expanding the material to V_{oo} along the measured release path. The experimental release path results do not extend to zero pressure, so V_{oo} was estimated by computing

an isentrope from the end of the measured release path to zero pressure. For the limestone shots the calcite VI parameters were used; for the chalk shots calcite I and II parameters were used (Table 3). This approximation leads to an underestimate of the integral term in equation (20), and therefore to an overestimate of ΔE_p. The assumed complete release densities and calculated post-shock energy increases are listed in Table 4. Figure 11 is a plot of post-shock energy increase ΔE_p as a function of shock pressure. Although the data are somewhat scattered, a trend toward higher post-shock energy content with increased pressure is observed. For the Solenhofen limestone ΔE_p reaches 300-400 J/g at about 25 GPa. For the Dover chalk shocked to 10 GPa, ΔE_p is about 1600 J/g. The curves in Figure 11 were calculated assuming isentropic release from the Hugoniot. For the Solenhofen limestone shots, the zero-pressure, isentropic release temperature T_{rel} was calculated using the parameters for calcite VI, whereas for the Dover chalk shots the calculation is based on the calcite I and calcite II parameters (Table 3). Because of the large amount of shock heating occurring upon compression of the initially porous chalk, post-shock energy and entropy values are only moderately sensitive to the choice of isentrope. The calculated post-shock energy gain ΔE_p was then obtained using

$$\Delta E_p = \int_{T_o}^{T_{rel}} C_v \, d\,T \qquad (21)$$

where T_o is the initial temperature and C_v is the calcite heat capacity at constant volume. The integration is carried out along the 1 bar isobar. C_v was calculated using the C_p (heat capacity at constant pressure) values of Robie *et al.* [1978]. The calculated values of post-shock energy content are in good agreement with the experimentally determined values.

The energy required for incipient decarbonation (volatilization) E_{IV} can be

calculated using the data of Robie *et al.* [1978]. It is important to bear in mind that the equilibrium of the reaction

$$CaCO_{3\,(calcite)} \rightleftarrows CaO_{(solid)} + CO_{2\,(gas)} \tag{22}$$

is strongly influenced by the ambient pressure of CO_2, P_{CO_2}. Thus for pure solid calcite and pure solid CaO, the Gibbs free energy of reaction (22) ΔG_{rx} is

$$\Delta G_{rx} = \Delta G^{o}_{rx} + RT\,ln\,P_{CO_2} \tag{23}$$

where the reference state for the solids is defined as pure solids at 1 bar pressure and the temperature of interest T, and for CO_2 the reference state is pure CO_2 gas at 1 bar (10^5 Pa) pressure and T. Thus for P_{CO_2} = 1 bar the temperature of incipient vaporization T_{IV} is approximately 1171 K and the energy of incipient vaporization E_{IV}, given by

$$E_{IV} = \int_{T_o}^{T_{IV}} C_{v\,(calcite)}\,dT \tag{24}$$

is approximately 980 J/g [Vizgirda and Ahrens, 1982; Kieffer and Simonds, 1980]. However, for $P_{CO_2} \approx 3.3\times10^{-4}$ bar (corresponding to dry air at 1 bar total pressure) T_{IV} is approximately 800 K, and E_{IV} is about 530 J/g, and for $P_{CO_2} \sim 4.3\times10^{-8}$ bar (corresponding to dry air at a total presure of 100 μm Hg) T_{IV} is about 596 K and E_{IV} is 296 J/g. Thus E_{IV} is strongly dependent on the explicit value of P_{CO_2} used in the calculation of T_{IV}, and conversely, the amount of CO_2 evolved during release may depend on the ambient P_{CO_2}.

Such equilibrium considerations do not apply absolutely in a dynamic shock experiment, but evidence that ambient CO_2 pressure affects the amount of evolved CO_2 comes from comparison of the work of Boslough *et al.* [1982] with that of Lange and Ahrens [1983] and that of Kotra *et al.* [1983]. The former

investigators studied the evolution of CO_2 during shock compression of calcite by capturing the evolved gas in an initially evacuated, confined chamber. For a shock pressure of 16 GPa only 0.03 to 0.3 per cent of the CO_2 was volatilized, and the final P_{CO_2} in the chamber at room temperature was between about 2.7×10^{-3} to 7.2×10^{-3} bars [M. Boslough, personal communication, 1984]. For $P_{CO_2} = 6 \times 10^{-3}$ bars, $T_{IV} = 900$ K and $E_{IV} = 648$ J/g. The studies of Lange and Ahrens [1983, 1984] were performed using vented assemblies [Lange and Ahrens, 1982]; therefore the final P_{CO_2} was that of air, 3.4×10^{-4} bar. For $P_{CO_2} = 3.4 \times 10^{-4}$ bar, $T_{IV} = 800$ K and $E_{IV} = 528$ J/g. They found significant decarbonation; as much as 30 per cent at pressures as low as 10 GPa (see Figure 12). The analytical method was different in each of the two sets of experiments; Boslough *et al.* determined the amount of CO_2 evolved whereas Lange and Ahrens determined the amount of CO_2 remaining in the recovered solid material. Nonetheless, it appears that at least part of the difference in results may be attributed to differences in P_{CO_2}. The results of Kotra *et al.* [1983] differ from those discussed above because their targets (both vented and non-vented) were exposed to the CO_2-rich muzzle gases from the gun barrel. The very low fraction of CO_2 volatilized as a function of shock pressure obtained by these workers may be caused by very high P_{CO_2} during release.

There are several implications of these results.

1. The release paths determined in this study may not be completely comparable to the volatilization results of either Boslough *et al.* or Lange and Ahrens, inasmuch as the experiments reported here were performed at about 100 μm air pressure ($P_{CO_2} \sim 4.3 \times 10^{-8}$bar).

2. The evolution of P_{CO_2} must be taken into account when calculating the evolution of impact-induced planetary atmospheric CO_2 content. Note also that

these considerations apply to the shock entropy criterion for vaporization upon release [Ahrens and O'Keefe, 1972; Zel'dovich and Raizer, 1967], because this method also depends on the identification of a T_{IV} for calculation of S_{IV} (entropy of incipient vaporization). Furthermore, the equilibrium considerations apply to any shock devolatilization process, especially shock dehydration [*c.f.* Boslough *et al.*, 1980; Lange and Ahrens, 1982].

The shock entropy criterion for incipient or complete vaporization [Zel'dovich and Raizer, 1967; Ahrens and O'Keefe, 1972] is convenient to use because it does not require experimental knowledge of the exact release path. Instead, the entropy gain in the shocked state ΔS_H is calculated according to

$$\Delta S_H = S_{tr} + C_v \ln (T_H / T_s) \tag{25}$$

where S_{tr} is the entropy of transition from calcite to calcite VI at 1 bar and 298 K and T_H and T_s are calculated by continuum methods (Zel'dovich and Raizer, 1967). The entropy of transition has been estimated to be between -.116 and -.086 J/g on the basis of entropy-molar volume systematics [Vizgirda and Ahrens, 1982] and we have adopted the value of -0.101 J/g for use here (Table 3). The shock entropy is dependent on T_H, which in turn is greatly influenced by the initial porosity of the material. Assuming isentropic release from the shocked state [Kieffer and Delaney, 1979; Jeanloz and Ahrens, 1979] the entropy of the completely released state will be equal to that of the shocked state, and this value is compared to the entropy of incipient vaporization S_{IV}, where

$$S_{IV} = \int_{T_o}^{T_{IV}} \frac{C_p}{T} dT \tag{26}$$

where C_p is the atmospheric pressure heat capacity at constant pressure, obtained from Robie *et al.* [1978]. As discussed above, T_{IV} will be dependent on

the P_{CO_2} chosen. The entropy of complete vaporization at T_{IV}, S_{cv}, is computed from the values of entropy as a function of temperature in Robie *et al.* [1978]. Figure 13 is a plot of shock entropy versus shock pressure for calcite of varying porosities calculated using the calcite Hugoniot of Adadurov *et al.* [1961] and the parameters for calcite VI listed in Table 3. The Hugoniots for the porous material are calculated according to

$$P_p = P_D \left\{1 - \frac{\gamma}{2}\left[\frac{V_{o,D}}{V_H} - 1\right]\right\} \Big/ \left\{1 - \frac{\gamma}{2}\left[\frac{V_{o,P}}{V_H} - 1\right]\right\} \qquad (27)$$

where P_p and P_D are the pressures at volume V_H of the porous material and the dense material, respectively, γ is the Gruneisen parameter, and $V_{o,p}$ and $V_{o,D}$ are the zero-pressure volumes of the porous and dense materials, respectively (Zel'dovich and Raizer, 1967). The experimentally determined shock entropies from this study are also plotted. The results for the Solenhofen limestone (initial porosity about .04) indicate that S_{IV} for $P_{CO_2} = 4.3 \times 10^{-8}$ bar (dry air atmosphere at 100 μm Hg total pressure, the conditions of the experiment) is reached at about 12-20 GPa, and that at about 25 GPa between 20-40% of the CO_2 would be volatilized. The results from the Dover chalk shots (initial porosity of 0.49) indicate that greater than 90% of the material would be decarbonated at 10 GPa shock pressure under the experimental conditions. For an air atmosphere ($P_{CO_2} = 3.3 \times 10^{-4}$ bar) the figure indicates a minimum pressure for incipient devolatilization of non-porous calcite of 21 to 32 GPa, compared with the experimental value of less than 10 GPa determined by Lange and Ahrens.

The shock energy or entropy criteria for incipient and complete vaporization when applied using the ambient (or final) vapor composition yield the lowest values of E_{IV} or S_{IV} and thus predict the greatest amount of devolatilization consistent with equilibrium thermodynamics. Thus, equilibrium thermodynamic

considerations fail to describe the experimental results for Solenhofen limestone even when the most generous assumptions concerning the final state of equilibrium are made.

We therefore conclude that a mechanism for the localization of thermal energy such as the shear instability model [Grady, 1977, 1980; Horie, 1980] is required to explain the experimental observations. In the case of single crystal calcite the existing shock temperature determinations support this conclusion. Kondo and Ahrens [1983] report a shock temperature of 3700K and an emissivity of 0.0025 for single crystal calcite shocked to 40 GPa. This temperature is several times the continuum temperature of 1300-1500K [Vizgirda and Ahrens, 1982]. Textural examination of recovered calcite shocked to 40 GPa suggests the presence of partially molten material into which shock released CO_2 has been injected [Lange and Ahrens, 1984]. Schmitt (personal communication) has measured a shock temperature of 2455 K for single crystal calcite shocked to 22.5 GPa.

The relationships between measured shock temperatures, calculated continuum temperatures release paths, and the calcite devolatilization equilibria are shown in Figure 14. This figure shows the P-T phase diagram for $CaCO_3$, the Hugoniot (continuum) P-T data for the Solenhofen limestone and Dover chalk reported here, and the measured shock temperatures of single crystal calcite of Schmitt (personal communication) and Kondo and Ahrens [1983]. The calcite VI liquid boundary is drawn through the two measured shock temperature values, but the conclusions drawn below do not depend critically on this particular placement of the boundary. Representative isentropic release paths, using the parameters in Table 3, are shown for several points. The diagram illustrates that the isentropic release paths of shocked non-porous carbonates (Solenhofen limestone), calculated using continuum temperatures, do not cross into the

$CaO_{(s)} + CO_{2\,(vapor)}$ field until very low pressures ($10^{-7} - 10^{-8}$ GPa) are reached. Shocked Dover chalk, particularly at shock pressures as high as 10 GPa, relaxes into the solid plus vapor region at pressures of $10^{-3} - 10^{-4}$ GPa. However, isentropic release from points corresponding to measured shock temperatures pass into the liquid field region at pressures of 10^{1} GPa or higher, into the liquid plus vapor field at pressures of 10^{-1} GPa or higher, and then into the solid plus vapor region at pressures of about 10^{-2} GPa. The high measured shock temperatures are related to shear banding phenomena, and it thus appears that localization of thermal energy is an integral part of the devolatilization process. The diagram also indicates that the effect of CO_2 pressure on the fraction devolatilized will be more modest in the case of shear band controlled devolatilization than in the case of devolatilization controlled by continuum temperatures.

Conclusions

Solenhofen limestone shocked into the calcite VI region retains its shear strength in the shocked state at pressures between about 12 and 20 GPa. Equilibrium thermodynamic calculation of the energy and entropy required for incipient devolatilization combined with measured values of the post-shock energy and entropy gain fail to quantitatively predict the amount of volatile loss upon release. This result indicates that inhomogeneous deformation processes occur in this pressure range. Therefore the density of the shear bands created in this shock-pressure interval must be insufficient to modify the bulk mechanical properties of the polystalline aggregate. The shear bands may be sites of initiation of partial melting and nucleation of evolved CO_2 upon release. At shock pressures above about 20 GPa loss of strength of the material may occur, implying that the shear band density is large enough to affect mechanical properties.

Isentropic release paths of material initially at the shock pressure and the measured shock temperature pass through the vapor plus liquid field into the

vapor plus solid field, giving further support to the conception that devolatilization is associated with shear band formation.

At shock pressures of ~10 GPa, Dover chalk (ρ_0 = 1.40 g/cm^3) appears to have lost its shear strength, but at 5 GPa the results are ambiguous. Post-shock entropy calculations indicate that greater than 90% of the CO_2 is devolatilized upon release from 10 GPa pressure.

Equilibrium calculations and experimental observations indicate that the amount of devolatilization of volatile-bearing minerals upon impact is dependent on the ambient partial pressure of the volatile species. The shock pressure required for incipient devolatilization increases with ambient volatile species partial pressure. This effect causes the range of planet sizes in which partial devolatilization of carbonates occurs to be larger than that calculated based on devolatilization experiments carried out in air [Lange and Ahrens, 1983, 1984]. Volatile release is enhanced relative to that calculated by Lange and Ahrens in the early stages of planetary accretion, when the atmosphere is sparse, and is inhibited in the later stages, when the atmosphere is relatively dense.

Acknowledgments. We thank E. Gelle, M. Long, W. Miller, and C. Manning for their help in performing these experiments. M. Boslough, S. Rigden, and B. Svendsen provided valuable insight and discussion. Research supported by NASA NGL-05-002-105. Contribution #4134, Division of Geological and Planetary Sciences, California Institute of Technology.

References

Adadurov, G. A. D., D. B. Balashov, and A. N. Dremin, A study of the volumetric compressibility of marble at high pressures, *Bull. Acad. Sci. USSR Geophys. Ser.*, *1961(5)*, 483-486, 1961.

Ahrens, T. J. and V. G. Gregson, Jr., Shock compression of crustal rocks: Data for quartz, calcite, and plagioclase rocks, *J. Geophys. Res.*, *69*, 4839-4874, 1964.

Ahrens, T. J., and J. T. Rosenberg, Shock Metamorphism: Experiments on quartz and plagioclase, in *Shock Metamorphism of Natural Materials*, edited by B. M. French and N. M. Short, pp. 59-81, Mono Book Corp., Baltimore, MD, 1968.

Ahrens, T. J., and J. D. O'Keefe, Shock melting and vaporization of lunar rocks and minerals, *The Moon*, *4*, 214-249, 1972.

Ahrens, T. J., J. L. Lower, and P. L. Lagus, Equation of state of forsterite, *J. Geophys. Res.*, *76*, 518-528, 1971.

Anderson, O. L., E. Schreiber, and R. C. Liebermann, Some elastic constant data on minerals relevant to geophysics, *Rev. Geophys.*, *6*, 491-524, 1968.

Baker, E. H., The calcium oxide-carbon dioxide system in the pressure range 1-300 atmospheres, *Chem. Soc. J.*, *1962*, 464-470, 1962.

Boslough, M. B., Shock-wave properties and high-pressure equations of state of geophysically important materials, Ph.D. thesis, California Institute of Technology, 1983.

Boslough, M. B., R. J. Weldon, and T. J. Ahrens, Impact-induced water loss from serpentine, nontronite, and kernite, Proc. Lunar Planet. Sci. Conf. *11th*, 2145-2158, 1980.

Boslough, M. B., T. J. Ahrens, J. Vizgirda, R. H. Becker, and S. Epstein, Shock-induced devolatilization of calcite, *Earth Planet. Sci. Lett.*, *61*, 166-170, 1982.

Boslough, M. B., and T. J. Ahrens, Shock wave properties of anorthosite and

gabbro, in press, 1984.

Bridgman, P. W., The high pressure behavior of miscellaneous minerals, *Am. Jour. Sci.*, *237*, 7-18, 1939.

Burdick, L., and D. L. Anderson, Interpretation of velocity profiles of the mantle, *J. Geophys. Res.*, *80*, 1070-1074, 1975.

Carlson, W. D., The polymorphs of $CaCO_3$ and the aragonite-calcite transformation, in *Carbonates: Mineralogy and Chemistry, Reviews in Mineralogy, Volume 11*, edited by R. J. Reeder, pp. 191-225, Mineralogical Society of America, Washington, D.C., 1983.

Courant, R., and K. O. Friedrichs, *Supersonic Flow and Shock Waves*, Interscience, New York, 1948.

Cowperthwaite, M., and R. F. Williams, Determination of constitutive relationships with multiple gauges in nondivergent flow, *J. Appl. Phys.*, *42*, 456-462, 1971.

Grady, D. E., Processes occurring in shock wave compression of rocks and minerals, in *High Pressure Research: Applications in Geophysics*, edited by M. H. Manghnani and S. Akimoto, pp. 389-438, Academic Press, New York, 1977.

Grady, D. E., Shock deformation of brittle solids, *J. Geophys. Res.*, *85*, 913-924, 1980.

Grady, D. E., Compression wave studies in Oakhall Limestone, Report *SAND83-0370*, Sandia Laboratories, 1983.

Grady, D. E., W. I. Murri, and G. R. Fowles, Quartz to stishovite: Wave propagation in the mixed phase region, *J. Geophys. Res.*, *79*, 332-338, 1974.

Grady, D. E., W. I. Murri, and P. S. DeCarli, Hugoniot sound velocities and phase transformations in two silicates, *J. Geophys. Res.*, *80*, 4857-4861, 1975.

Grady, D. E., R. E. Hollenbach, K. W. Schuler, and J. F. Callender, Compression

wave studies in Blair dolomite, Report *SAND 76-0005*, Sandia Laboratories, 1976.

Grady, D. E., R. E. Hollenbach, and K. W. Schuler, Compression wave studies on calcite rock, *J. Geophys. Res.*, *83*, 2839-2849, 1978.

Grieve, R. A. F., and P. B. Robertson, The terrestrial cratering record, 1, current status of observations, *Icarus*, *83*, 212-229, 1979.

Horie, Y., Thermodynamics of dislocations and shock compression of solids, *Phys. Rev. B*, *21*, 5549-5557, 1980.

Huang, W.-L., and P. J. Wyllie, Melting relations in the systems CaO-CO_2 and MgO-CO_2 to 33 kilobars, *Geochim. Cosmochim. Acta*, *40*, 129-132, 1976.

Hughes, D. S., and J. H. Cross, Elastic wave velocities in rocks at high pressures and temperatures, *Geophysics*, *16*, 577-593, 1951.

Irving, A. J., and P. J. Wyllie, Melting relationships in CaO-CO_2 and MgO–CO_2 to 36 kilobars with comments on CO_2 in the mantle, *Earth Planet. Sci. Lett.*, *20*, 220-225, 1973.

Jamieson, J. C., Introductory studies of high-pressure polymorphism to 24,000 bars by x-ray diffraction with some comments on calcite II, *J. Geol.*, *65*, 334-343, 1957.

Jeanloz, R., and T. J. Ahrens, Release adiabat measurements on minerals: The effect of viscosity, *J. Geophys. Res.*, *84*, 7545-7548, 1979.

Kalashnikov, N. G., M. N. Pavlovskiy, G. V. Simakov, and R. F. Trunin, Dynamic compressibility of calcite-group minerals, *Bull. Acad. Sci. USSR Phys. Solid Earth*, *1973(2)*, 80-84, 1973.

Kieffer, S. W., and J. W. Delaney, Isentropic decompression of fluids from crustal and mantle pressures, *J. Geophys. Res.*, *84*, 1611-1620, 1979.

Kieffer, S. W., and C. H. Simonds, The role of volatiles and lithology in the impact cratering process, *Rev. Geophys. Space Phys.*, *18*, 143-181, 1980.

Kondo, K., and T. J. Ahrens, Heterogeneous shock-induced thermal radiation in minerals, *Phys. Chem. Minerals*, *9*, 173-181, 1983.

Kotra, R. K., T. H. See, E K. Gibson, F. Horz, M. J. Cintala, and R. S. Schmidt, Carbon dioxide loss in experimentally shocked calcite and limestone, *Lunar and Planetary Science*, *14*, 401-402, 1983.

Lange, M. A., and T. J. Ahrens, Impact induced dehydration of serpentine and the evolution of planetary atmospheres, *J. Geophys. Res.*, *87*, A451-A456, 1982.

Lange, M. A., and T. J. Ahrens, Shock-induced CO_2-production from carbonates and a proto-CO_2-atmosphere on the Earth, *Lunar and Planetary Science*, *14*, 419-420, 1983.

Lange, M. A., and T. J. Ahrens, CO_2 loss in shock-loaded calcite and implications for primary atmospheres, in preparation, 1984

Larson, D. B., and G. D. Anderson, Plane shock wave studies of porous geologic media, *J. Geophys. Res.*, *84*, 4592-4600, 1979.

Marsh, S. P., editor, *LASL Shock Hugoniot Data*, University of California Press, Berkeley, Calif., 1980.

McQueen, R. G., S. P. Marsh, and J. N. Fritz, Hugoniot equation of state of twelve rocks, *J. Geophys. Res.*, *72*, 4999-5036, 1967.

McQueen, R. G., S. P. Marsh, J. W. Taylor, J. N. Fritz, and W. J. Carter, The equation of state of solids from shock wave studies, in *High-Velocity Impact Phenomena*, edited by R. Kinslow, pp. 293-417, Academic Press, New York, 1970.

Murri, W. J., D. E. Grady, K. D. Mahrer, Equation of state of rocks, *Final Report PYU-1883*, Stanford Research Institute, Menlo Park, Calif., 1975.

Peselnick, L., Elastic constants of Solenhofen limestone and their dependence on density and saturation, *J. Geophys. Res.*, *67*, 4441-4448, 1962.

Peselnick, L. and W. H. Wilson, Wave velocities and hysteresis in Solenhofen

limestone for pressures up to 12 kilobars, *J. Geophys. Res.*, *73*, 3271-3280, 1968.

Peterson, C. F., W. J. Murri, and M. Cowperthwaite, Hugoniot and release-adiabat measurements for selected geologic materials, *J. Geophys. Res.*, *75*, 2063-2072, 1970.

Robie, R. A., B. S. Hemingway, and J. R. Fisher, Thermodynamic properties of minerals and related substances at 298.15K and 1 bar (10^5 pascals) pressure and at higher temperatures, *Geological Survey Bull. 1452*, U. S. Geological Survey, Washington, D. C., 1978.

Sammis, C., D. L. Anderson, and T. Jordan, Application of isotropic finite strain theory to ultrasonic and seismological data, *J. Geophys. Res.*, *75*, 4478-4480, 1970.

Schuler, K. W., and D. E. Grady, Compression wave studies in Solenhofen Limestone, Report *SAND76-0279*, Sandia Laboratories, 1977.

Singh, A. K., and G. C. Kennedy, Compression of calcite to 40 kbar, *J. Geophys. Res.*, *79*, 2615-2622, 1974.

van Thiel, M., J. Shaner, and E. Salinas, Report UCRL *50108*, Vol. 3, Lawrence Livermore Laboratory, 1977.

Vizgirda, J., and T. J. Ahrens, Shock compression of aragonite and implications for the equation of state of carbonates, *J. Geophys. Res.*, *87*, 4747-4758, 1982.

Wang, C., and M. Meltzer, Propagation of sound waves in a rock undergoing phase transformations, *J. Geophys. Res.*, *78*, 1293-1298, 1973.

Zel'dovich, Ya., B., and Yu. P. Raizer, *Physics of Shock Waves and High-Temperature Hydrodynamic Phenomena*, Vol. II, Academic Press, New York, 1967.

Table 1. Summary of Intermediate, State, Hugoniot State, and Release Path Release Transition Data

				Shock States*				Release Path Phase Transitions		
Shot#	Projectile	Projectile Velocity V_p km/sec	Initial Density ρ_o g/cm^3	Shock Velocity U_s km/sec	Particle Velocity u_p km/sec	Pressure P GPa	Density ρ g/cm^3	Particle Velocity u_{p1} km/sec	Pressure P_1 GPa	Density ρ g/cm^3
				Solenhofen Limestone						
590	Al_2O_3	2.209 ±.017	2.591 ±.010	5.819 ±.150	1.467 ±.018	22.41 ±.44	3.480 ±.042	2.44 ±.10	6.48 ±1.27	2.90 ±.08
596	Fused quartz	2.158 ±.02	2.584 ±.009	(4.60) ±.08	(0.030) ±.010	(0.36) ±.12	(2.601) ±.021	1.26 ±.03	8.20 ±.60	3.11 ±.02
				(4.415) ±.435	(0.40) ±.10	(4.58) ±1.05	(2.641) ±.079			
				5.081 ±.080	0.997 ±.015	13.10 ±.16	3.215 ±.021			
598	Al_2O_3	2.310 ±.150	2.584 ±.010	6.073 ±.120	1.538 ±.110	24.14 ±1.67	3.461 ±.085	2.65 ±.06	3.21 ±.80	2.87 ±.04
600	Al_2O_3	1.965 ±.005	2.608 ±.002	5.741 ±.008	1.319 ±.004	19.75 ±.06	3.386 ±.004	2.11 ±.04	4.97 ±.51	2.95 ±.03
602	Fused quartz	1.992 ±.010	2.604 .005	(5.706) ±.300	(0.030) ±.010	(0.45) ±.15	(2.618) ±.021	1.34 ±.04	5.97 ±.47	3.00 ±.02
				(4.774) ±.09	(0.200) ±.02	(2.56) ±.30	(2.715) ±.025			
				4.903 ±.050	0.936 ±.008	11.96 ±.09	3.219 ±.013			
				Dover Chalk						
599	Al_2O_3	2.078 ±.015	1.434 ±.030	3.750 ±.100	1.745 ±.018	9.39 ±.26	2.683 ±.085			
601	Al_2O_3	2.331 ±.020	1.434 ±.030	3.845 ±.050	1.959 ±.020	10.80 ±.22	2.924 ±.066			
620	Al_2O_3	1.619 ±.019	1.365 ±.024	2.933 ±.047	1.414 ±0.18	5.66 ±.13	2.635 ±.064			
622	Al_2O_3	2.235 ±.022	1.365 ±.024	3.652 ±.127	1.900 ±.023	9.47 ±.32	2.846 ±.131			

*Highest pressure state is final shock state. All others are intermediate states.

Values in parentheses are less reliable data.

Table 2. Summary of Polycrystalline Calcite Hugoniot Data

Material	Reference	ρ_o, g/cm^3	C_o, km/sec	s	Pressure Range, GPa
Solenhofen limestone	this work	2.594	3.269	1.796	12-24
Dover chalk	this work	1.40	.67	1.60	5-11
Polycrystalline calcite	Adadurov et al., 1961	2.703	3.40	2.00	5-13
			3.99	1.32	13-51
Polycrystalline calcite	Kalashnikov et al., 1973	2.665	3.70	1.44	10-94
		2.020	1.74	1.61	13-71
		1.706	1.15	1.60	10-59
Solenhofen limestone	van Thiel et al., 1977	2.585	3.62	1.39	6-90

Table 3. Properties of the Calcite Polymorphs

	I	II	III	VI
Zero-pressure density (300 K) ρ_o, g/cm^3	2.71[a]	2.71[a]	2.71[a]	3.0-3.1[b]
Bulk modulus K, GPa	71.1[a]	14.7[a]	51.7[a]	75-95[b]
$dK/dP = K'$	4.15[a]	4.62[a]	8.28[a]	4.1-3.5[b]
Transition energy E_{tr}, J/g	–	–	–	200-20[b]
Gruneisen parameter γ	1.5 $(V/V_o)^c$	1.5 $(V/V_o)^c$	1.5 $(V/V_o)^c$	1.5 $(V/V_o)^c$
Poisson's ratio σ	0.25[c]	0.25[c]	0.25[c]	0.25[c]
$K_{oo} \cdot d \ln V_p / dP = D_p$	2.13[e]	0.44[e]	1.55[e]	1.0-1.6[d]
$K_{oo} \cdot d \ln V_s / dP = D_s$	2.13[e]	0.44[e]	1.55[e]	1.0-0.1[d]
dV_p/dT, km/sec·K	-3×10^{-4} [d]	-3×10^{-4} [d]	-3×10^{-4} [d]	-3.3×10^{-4} [d]
dV_s/dT, km/sec·K	-3×10^{-4} [d]	-3×10^{-4} [d]	-3×10^{-4} [d]	-2.4×10^{-4} [d]
Specific heat capacity C_v, J/g·K	1.25[f]	1.25[f]	1.25[f]	1.25[f]

[a] Singh and Kennedy, 1974
[b] Vizgirda and Ahrens, 1982
[c] assumed
[d] Anderson *et al.*, 1968; Sammis *et al.*, 1970
[e] Peselnick and Wilson, 1968; Wang and Meltzer, 1973
[f] Dulong-Petit value, $T \gtrsim 650$; Vizgirda and Ahrens, 1982

Table 4. Calculated continuum Hugoniot temperatures T_H, extrapolated complete release density ρ_{oo}, and post-shock energy increase ΔE_p

Shot	T_H, K	ρ_{oo}, g/cm^3	ΔE_p, erg/g x10^{-9}
		Solenhofen Limestone	
602	551± 82	2.68±.02	1.11± .10
596	648± 31	2.81±.03	2.51± .16
600	825± 94	2.68±.03	2.40± .06
590	945±100	2.59±.10	2.15± .63
598	1024± 98	2.77±.03	4.46± .31
		Dover Chalk	
620	1089± 40	2.44±.02	9.13± .50
622	1747± 98	2.55±.03	16.21±1.26
601	1832± 97	–	–

Figure Captions

Figure 1. Schematic diagram of particle velocity gauge experiment. Top view, active element of foil gauge is oriented in and out of plane of page. Gauges are epoxied between plates of Solenhofen limestone and their electrical leads each go to an oscilloscope. Impact-induced velocity of gauge generates a voltage which is proportional to the magnetic field (generated by the Helmholtz coils). Pin signal triggers oscilloscopes.

Figure 2. Chalk (porous calcite) target assembly. Electrical leads from gauges and pins are omitted for clarity.

Figure 3. Schematic diagram of current-generating and signal-measuring circuits. Only one of four signal circuits are shown.

Figure 4. Particle velocity versus time after impact for shot 600 obtained from digitized voltage versus time oscilloscope records. Gauge 1 is nearest to impacted surface, gauge 4 is at free surface. Shock velocity was 5.741 km/sec, Hugoniot particle velocity was 1.319 km/sec, and shock pressure was 19.75 GPa.

Figure 5. Position-time (x-t) diagram of a particle velocity experiment. Projectile approaches from left and impacts stationary target at x=0, t=0. The diagram shows the (undesirable) case in which gauge 1 is intercepted by the rarefaction propagating forward from the projectile rear surface before arrival of rarefaction from rear surface.

Figure 6. Shock wave velocity U_s versus particle velocity u_p data for experiments reported here and comparison with previous results. Filled symbols show

present data for the Solenhofen limestone, open symbols show data for Dover chalk. Crosses with no symbol represent intermediate states. Lines represent fits of form $U_s = Co + s\,u_p$. Parameters for fits are listed in Table 2. Curves are labelled as follows: 1-Solenhofen limestone, this study, $\rho_o = 2.594$; 2-single crystal aragonite, [Vizgirda and Ahrens, 1982], $\rho_o = 2.93$; 3-polycrystalline calcite, [Adadurov *et al.*, 1961], $\rho_o = 2.703$; 4-Solenhofen limestone, [van Thiel *et al.*, 1977], $\rho_o = 2.585$; 5-polycrystalline calcite [Kalashnikov *et al.*, 1973], $\rho_o = 2.665$; 6-polycrystalline calcite, [Kalashnikov *et al.*, 1973], $\rho_o = 2.02$; 7-polycrystalline calcite, [Kalashnikov *et al.*, 1973], $\rho_o = 1.705$; 8-Dover chalk, this study, $\rho_o = 1.40$. Units of density, g/cm^3.

Figure 7. Hugoniot states and release paths for Solenhofen limestone and Dover chalk. Filled symbols are for Solenhofen limestone, open symbols are for Dover chalk, boxes represent initial densities. Heavy solid lines are fits to data (Table 2).

Figure 8. Particle velocity versus time after impact for shot 596, showing multiple shock fronts on leading edge of record (including HEL), and indicating presence of an intermediate release state during unloading.

Figure 9. Eulerian sound speeds, C_E, on the Hugoniot of shocked Solenhofen limestone. Ranges of compressional wave velocity V_p and bulk sound speed V_ϕ for calcite VI are computed using Eulerian finite strain theory (see text) and parameters listed in Table 3. Values plotted are for an isentrope originating at 750 K at zero pressure. Dashed line is V_ϕ along the Hugoniot of calcite VI calculated according to equation (18).

Figure 10. Eulerian sound speeds C_E on Hugoniot of Dover chalk. Solid and dashed lines represent compressional wave velocities and bulk sound velocities, respectively, of calcite polymorphs along a 750 K isentrope calculated using the parameters in Table 3. Roman numerals refer to the assumed calcite polymorph. Dotted line labelled H represents bulk sound speed along low pressure (5-13 GPa) polycrystalline calcite Hugoniot of Adadurov *et al.*, [1961] (Table 2) using equation (18).

Figure 11. Post-shock energy increase ΔE_p as a function of shock pressure. Also shown is energy of incipient vaporization E_{IV} calculated for several values of P_{CO_2}. 'STP air' refers to P_{CO_2} in dry air, 3.3×10^{-4} bars; 'Tank' refers to P_{CO_2} in impact tank under shot conditions, about 4.3×10^{-8} bars. Hatched regions represent values of ΔE_p calculated using calcite VI parameters (Table 3) for Solenhofen limestone and calcite I and II parameters for Dover chalk. The Hugoniot pressure of the porous material was calculated using equation (27).

Figure 12. Shock-induced CO_2 loss as a function of shock pressure in calcite as determined in experimentally shock loaded single crystal calcite in an ambient atmosphere of air. Data are from Lange and Ahrens [1984]. Also shown are CO_2 losses calculated using shock entropy method for various values of ambient CO_2 pressure. 'Tank' refers to the ambient CO_2 pressure in impact tank, about 4.3×10^{-8} bars; 'STP air' refers to the P_{CO_2} in dry air at standard temperature and pressure conditions, about 3.3×10^{-4} bars; Solid lines refer to the following combination of parameters of calcite VI; ρ_o = 3.1 g/cm^3, K_φ = 95 GPa, K' = 3.5, E_{trans} = 20 J/g. For dashed lines ρ_o = 3.0 g/cm^3, K_φ = 75 GPa, K' = 4.1, E_{trans} = 200 J/g.

Figure 13. Shock entropy as a function of shock pressure. The curves for porous calcite are calculated using the calcite Hugoniot of Adadurov *et al.* [1961], the correction for porosity embodied in equation (27), and the equation of state parameters for calcite VI listed in Table 3. S_{CV} and S_{TV} are calculated as a function of P_{CO_2} as described in text.

Figure 14. $CaCO_3$ phase diagram showing schematic paths of isentropic decompression from shocked states. The P-T phase diagram is based on the results of Carlson [1983], Huang and Wyllie [1976], Irving and Wyllie [1973], Baker [1962], and Jamieson [1957]. Stability fields of each polymorph are labelled with the appropriate roman numeral. The range of Hugoniot and release path temperatures for Solenhofen limestone are calculated using the range of values of properties of calcite VI (Table 3). Hugoniot and representative release path temperatures of Dover chalk are based on the low pressure calcite properties (Table 3). Open squares are shock temperature measurements on single crystal calcite by Kondo and Ahrens [1983] (K & A) and by Schmitt (personal communication, 1984; S). The representative isentropic release path for the point S is calculated using the calcite VI physical property data. Note that 10^{-4} GPa corresponds to 1 bar pressure. Q_1 is the invariant point, at which $CaCO_{3(s)}$, $CaO_{(s)}$, $CO_{2(vapor)}$, and liquid coexist. $CaCO_3$ melts incongruently between points Q_1 and Q_2, and melts congruently at pressures higher than Q_2. Metastable calcite II and III fields are separated by dashed lines. Extrapolated or inferred phase boundaries are shown by dash-dot lines. Dotted line represents the aragonite $\rightleftarrows$ calcite VI phase boundary constrained to lie below the limestone Hugoniot. Error bar on the dotted line represents the position of the line calculated using the range of property values for calcite VI listed in Table 3.

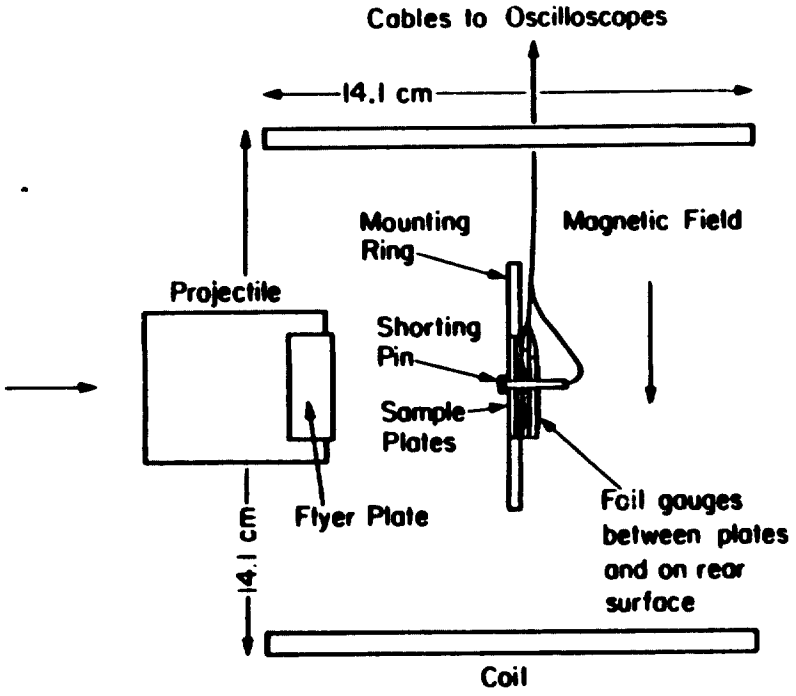

Top View

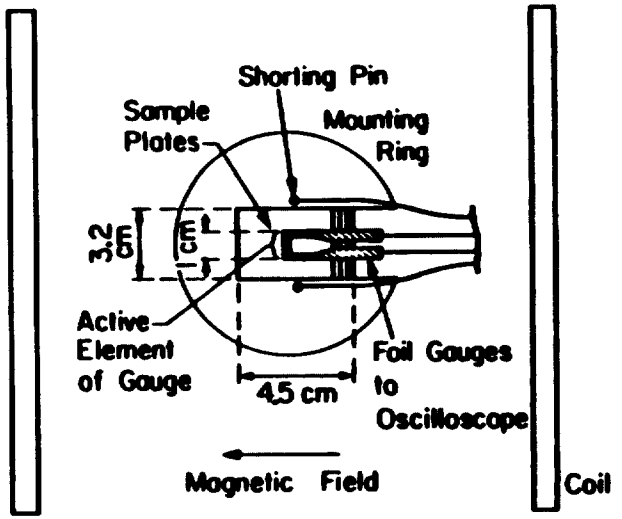

Rear View

FIGURE 1

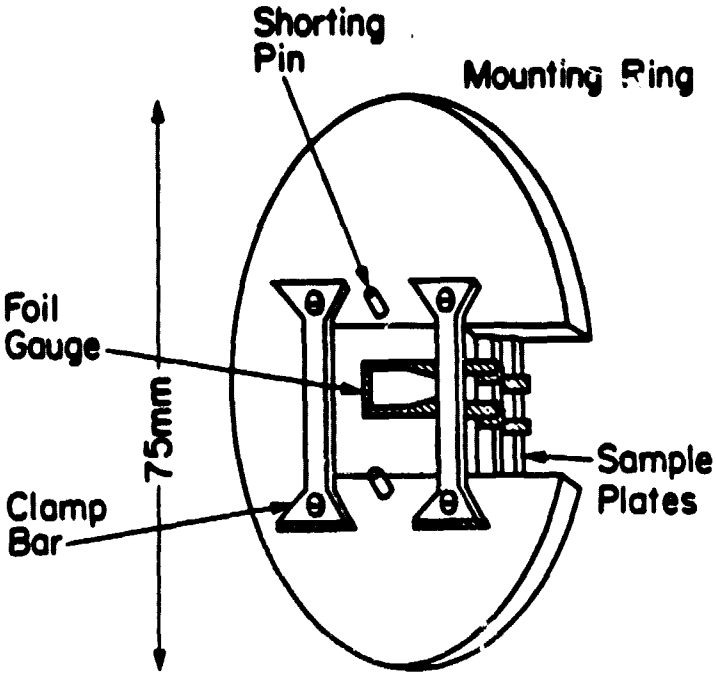

Rear View

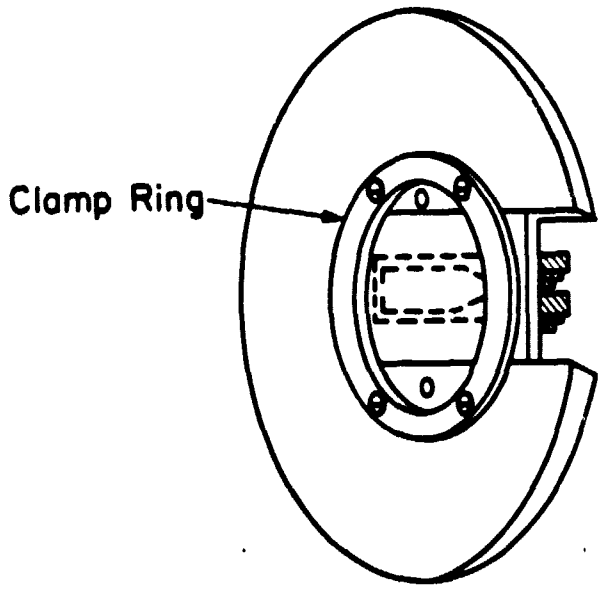

Front View

FIGURE 2

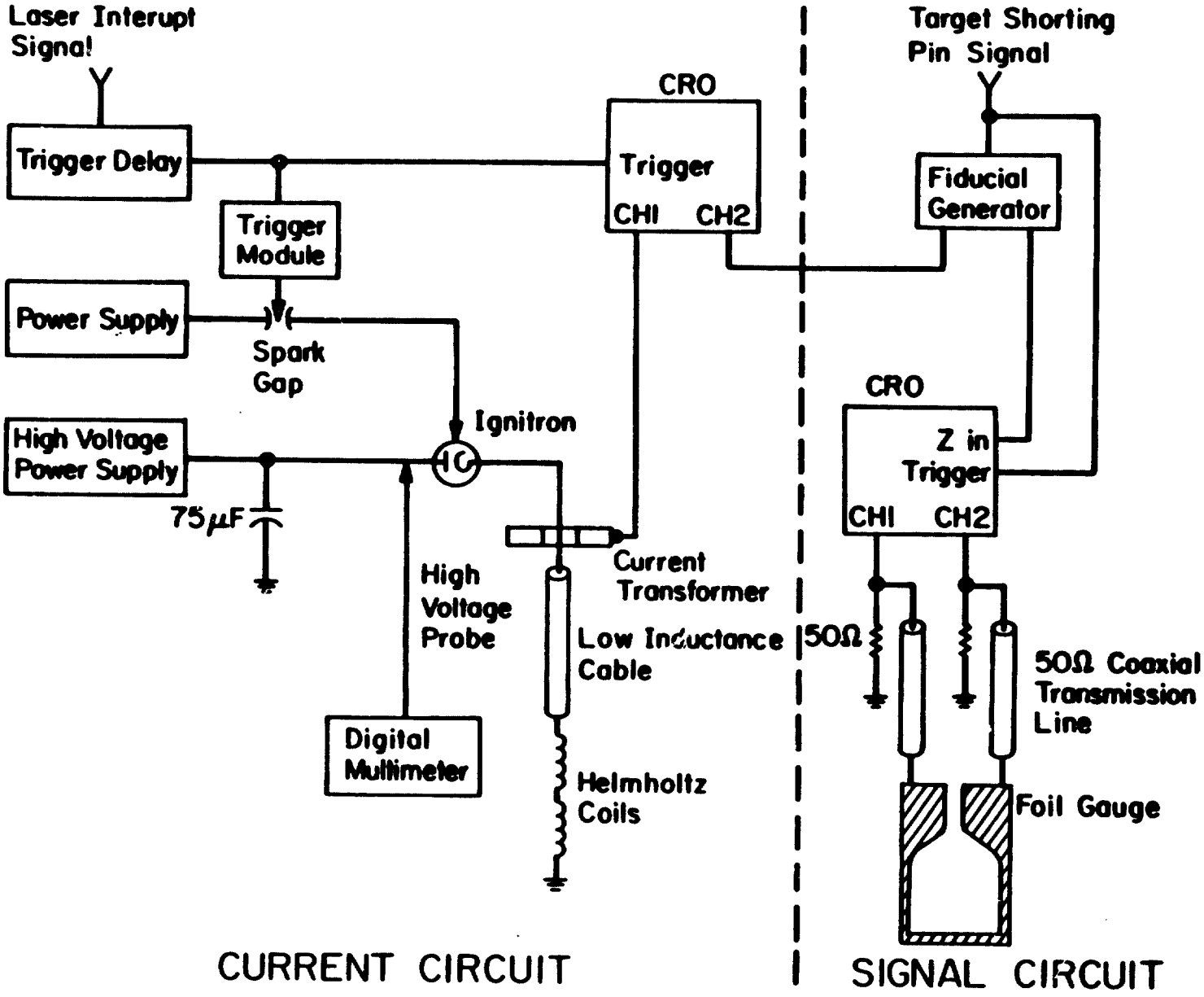

FIGURE 3

TJA84136MFD

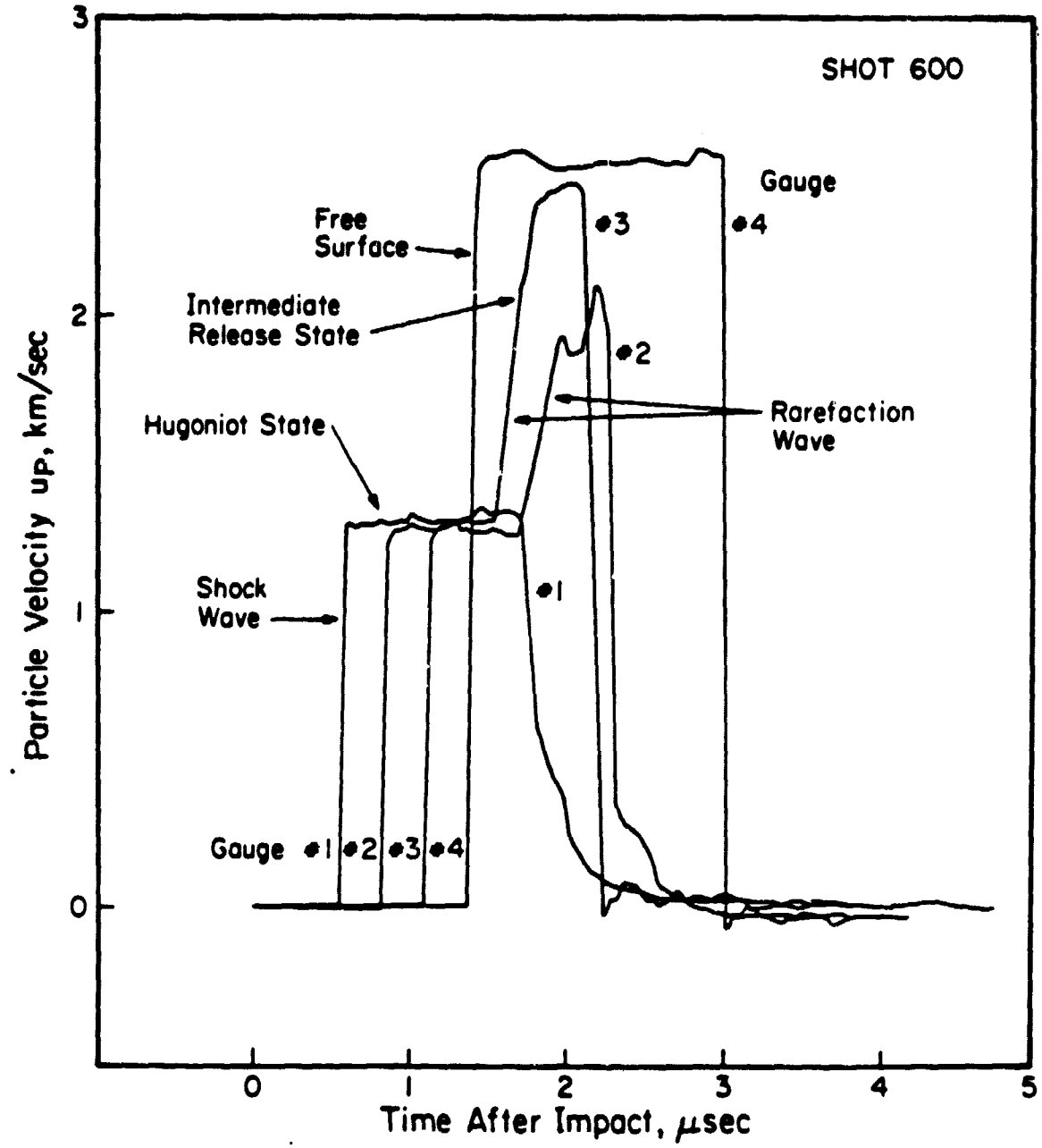
SHOT 600
Gauge
Free
Surface
#3
#4
Intermediate
Release State
#2
Rarefaction
Wave
Hugoniot State
Shock
Wave
#1
Gauge #1 #2 #3 #4
Particle Velocity up, km/sec
Time After Impact, μsec
0
1
2
3
4
5

FIGURE 4

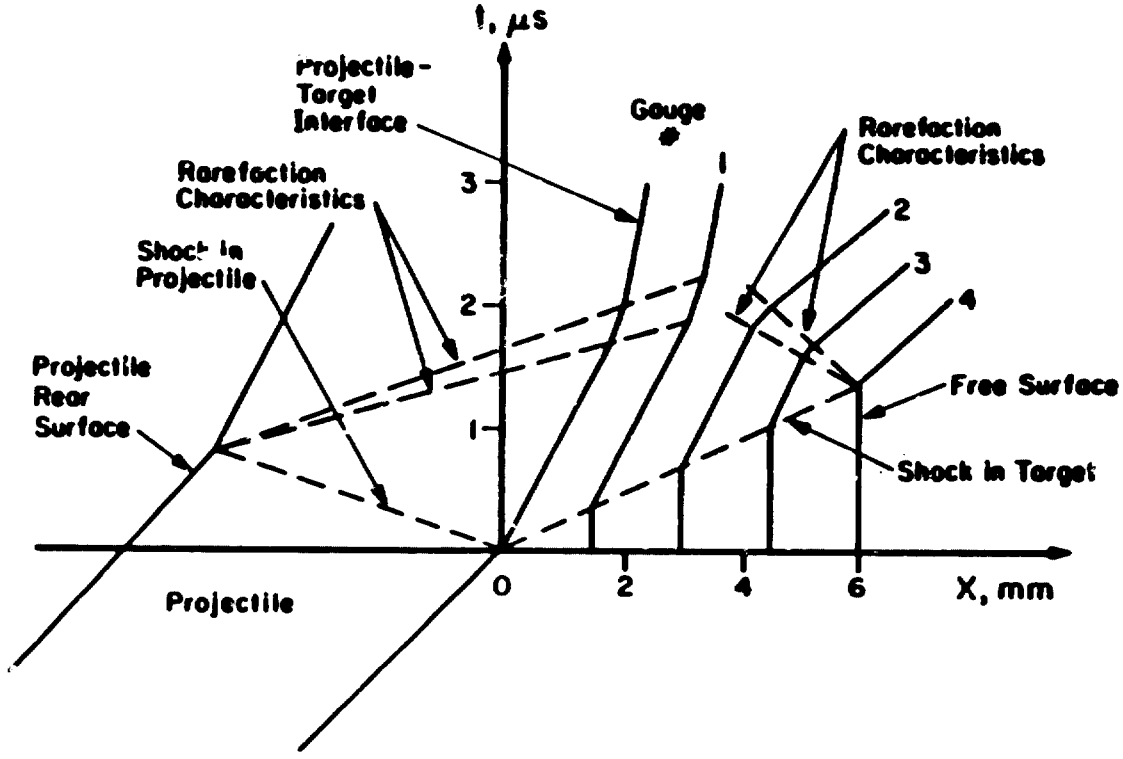
t, μs
Projectile-
Target
Interface
Gauge
#
Rarefaction
Characteristics
Rarefaction
Characteristics
Shock in
Projectile
Projectile
Rear
Surface
Free Surface
Shock in Target
Projectile
0
2
4
6
X, mm
1
2
3
4
1
2
3

FIGURE 5

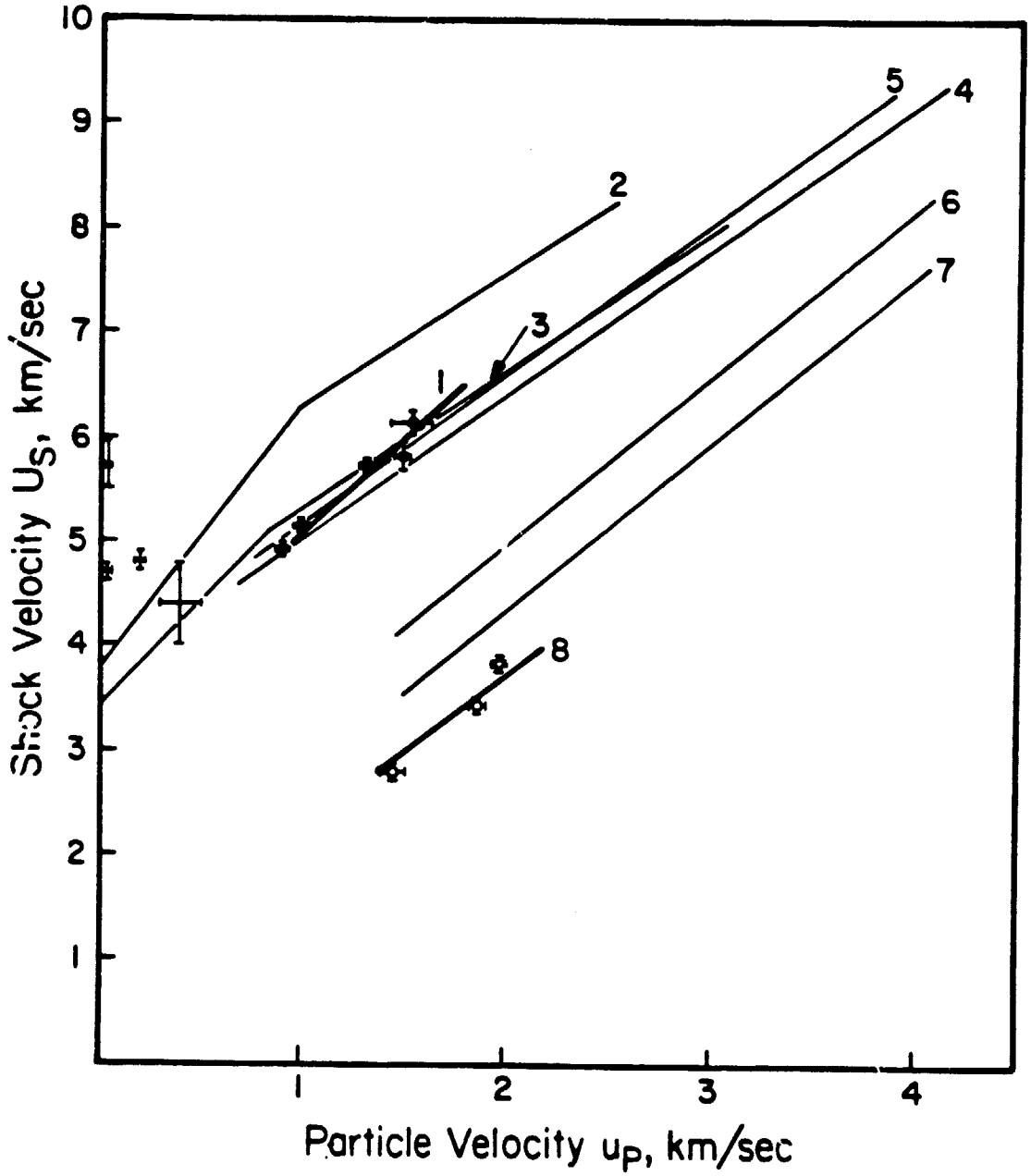
Shock Velocity U_S, km/sec
Particle Velocity u_P, km/sec
10
9
8
7
6
5
4
3
2
1
1
2
3
4
1
2
3
4
5
6
7
8

FIGURE 6

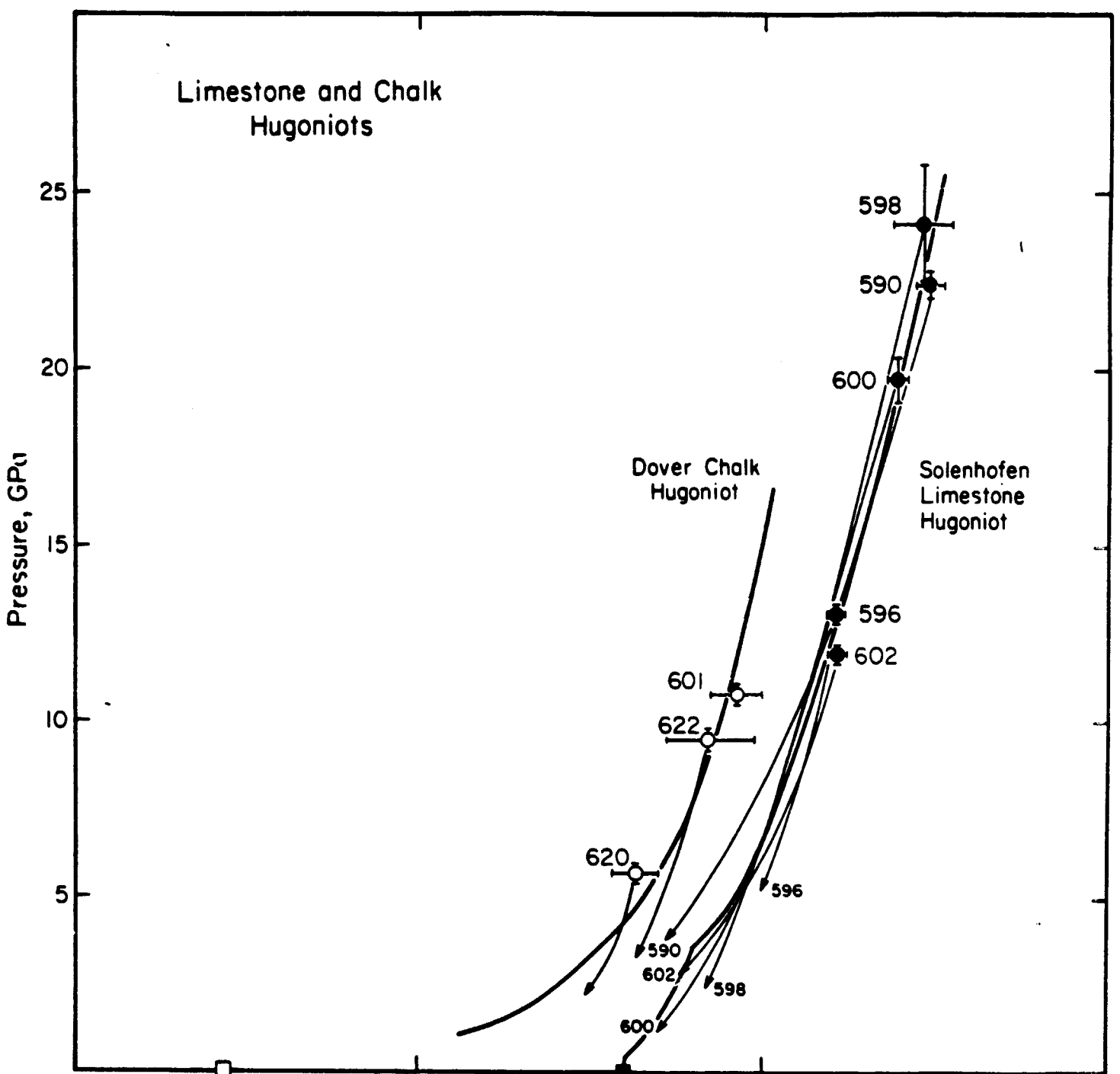

FIGURE 7

TJA84140LFD

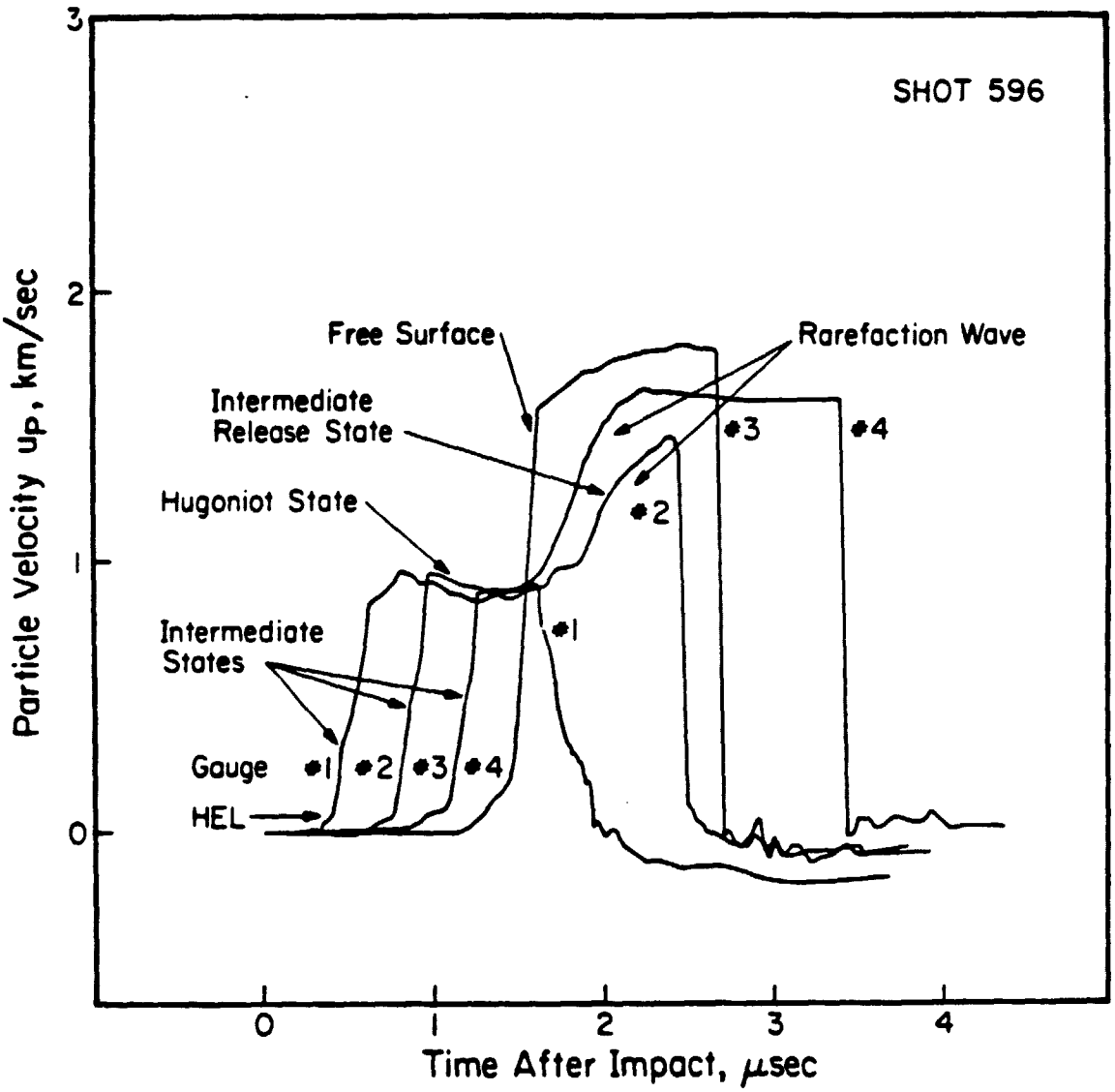
SHOT 596
Particle Velocity u_p, km/sec
Time After Impact, μsec
Free Surface
Rarefaction Wave
Intermediate Release State
Hugoniot State
Intermediate States
Gauge #1 #2 #3 #4
HEL
#1
#2
#3
#4
0
1
2
3
4

FIGURE 8

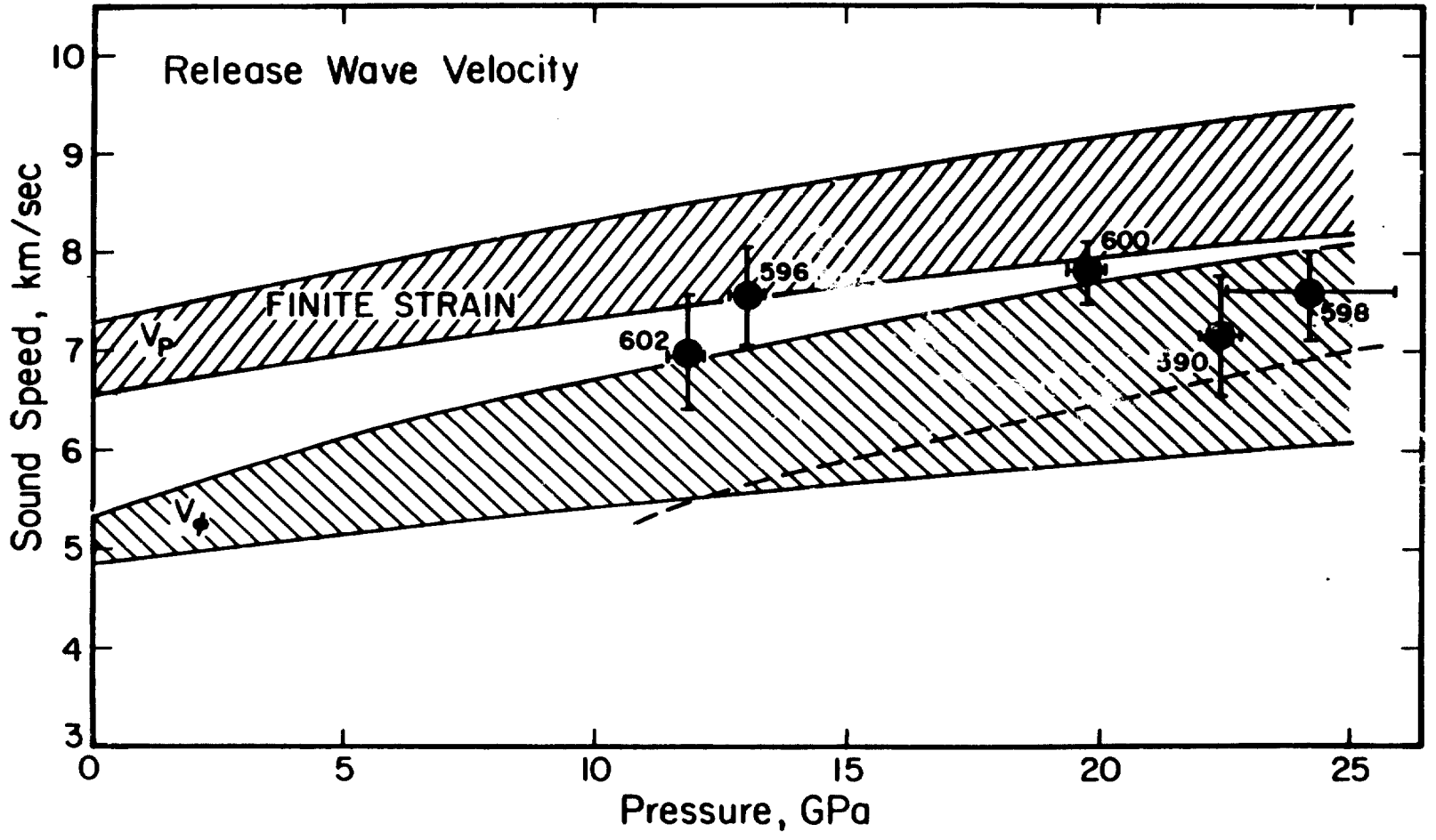

Figure 9

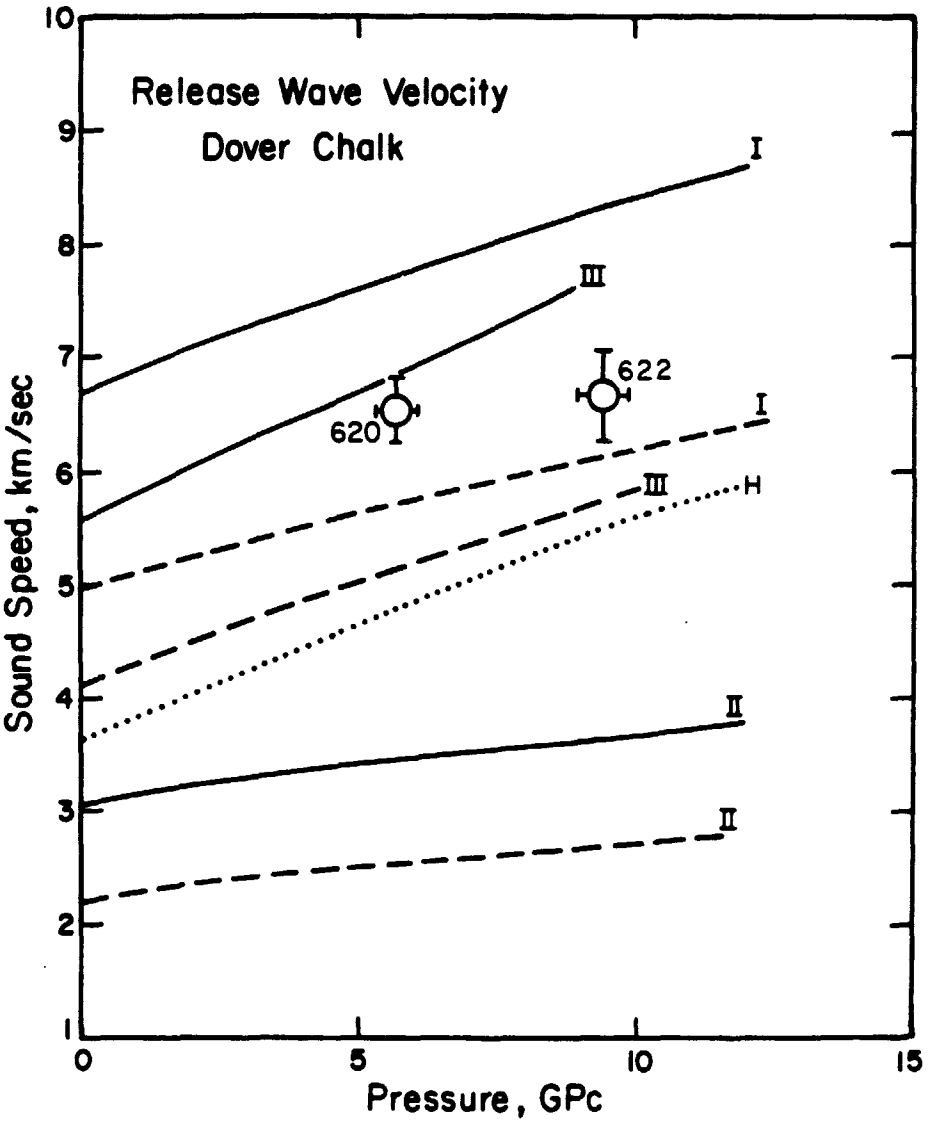
Release Wave Velocity
Dover Chalk
Sound Speed, km/sec
Pressure, GPc
I
III
II
H
620
622
10
9
8
7
6
5
4
3
2
1
0
5
10
15

Figure 10

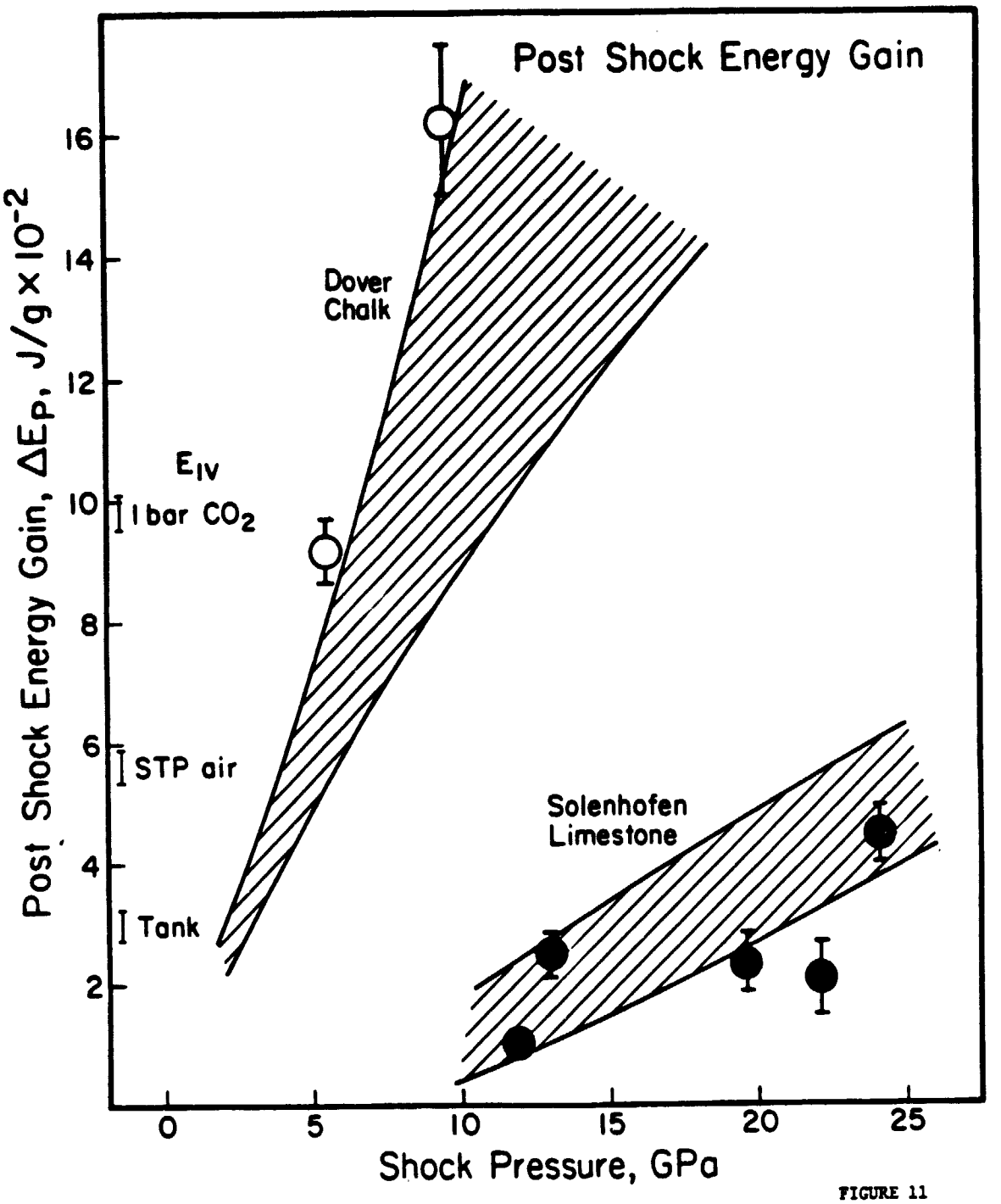

FIGURE 11

TJA84145MFD

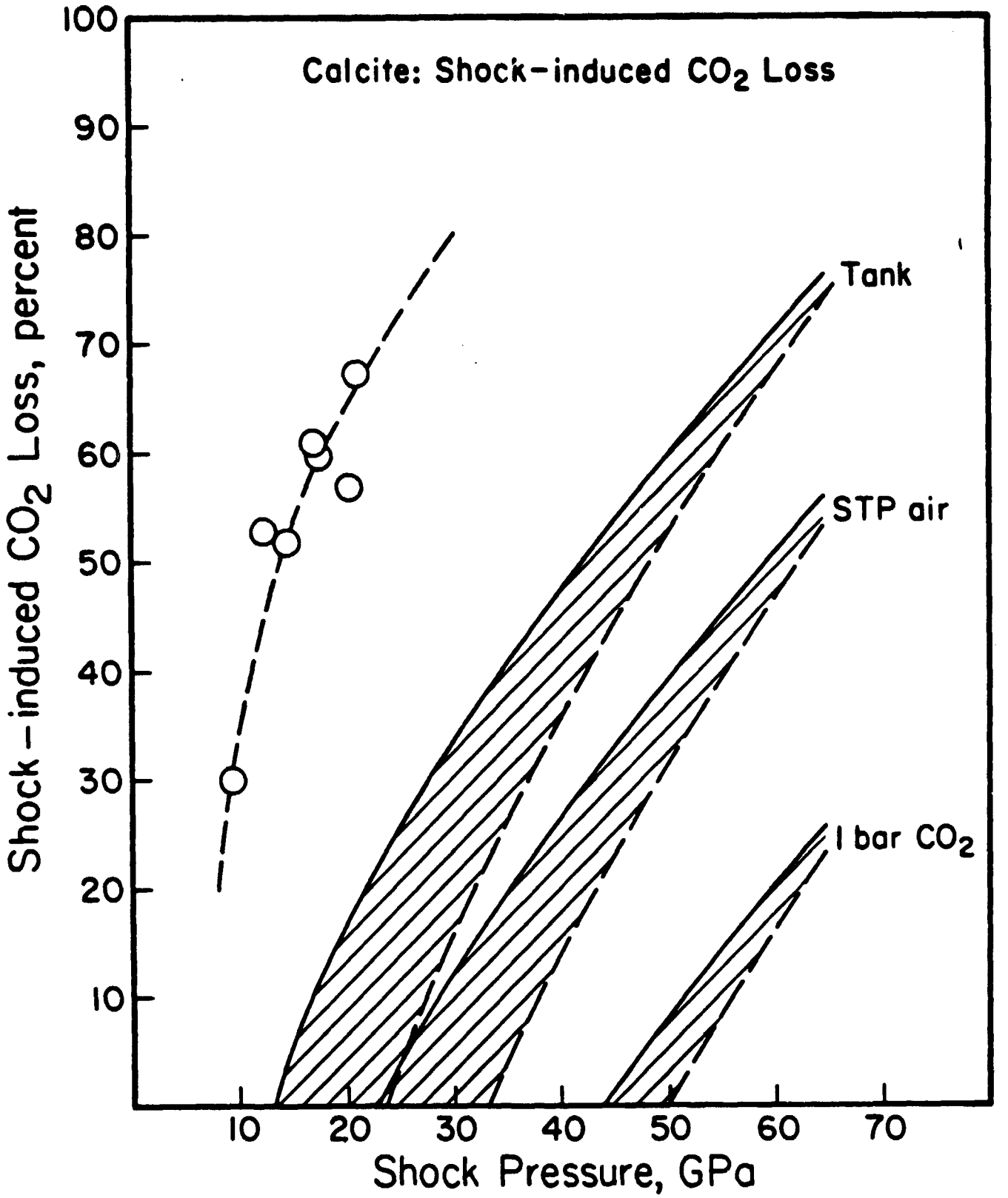

TJA84144SFD

FIGURE 12

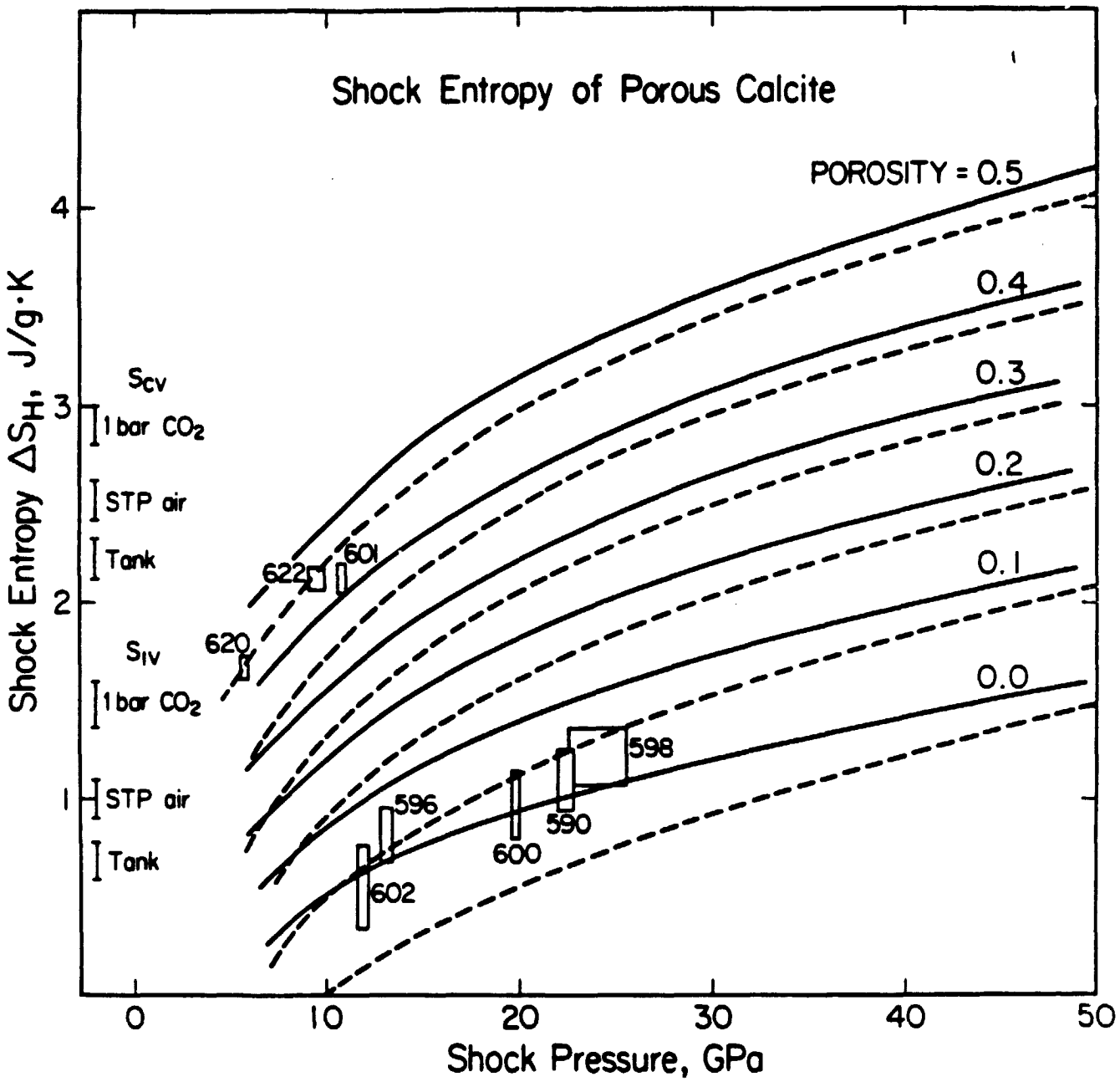

FIGURE 13

TJA84146LFD

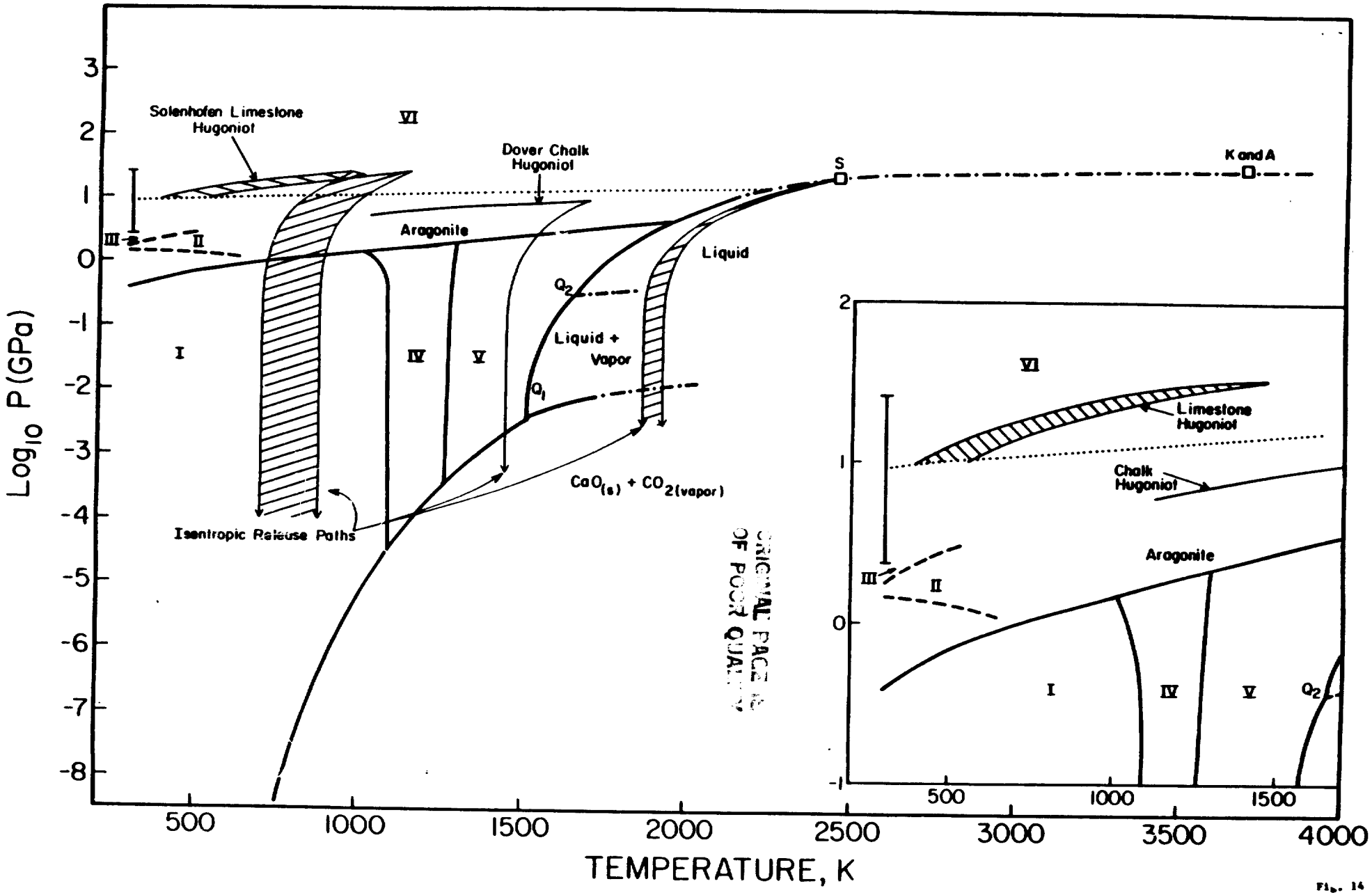

Fig. 14